Thesis Title

Silicon Slot Waveguide Based Optical Sensor

Supervisor

Dr. Mohammed Moseeur Rahman

Assistant Professor and Chairperson

Department Of Electronic and Communication Engineering

Submitted By:

Arifur Rahman

Id.2014-1-55-008

Md. Abdul Momin

Id. 2015-3-55-012

Md.Tuhin Sardar

Id.2015-3-55-014

Declaration

We hereby declare that we have completed our thesis on the topic entitled silicon slot waveguide based Optical Sensor. We have prepared this thesis and submitted to the Department of Electronics and Communications Engineering. This thesis is submitted to fulfill the requirement of the degree B.Sc. in Electronic and Telecommunication Engineering.

We claim that this work is done by our own. We also declare that this work has not been submitted anywhere for publication.

Signature: Signature:

Arifur Rahman

ID: 2014-1-55-008

Md.Abdul Momin

ID: 2015-3-55-012

Signature:

Tuhin Sardar

ID: 2015-3-55-014

Signature of Supervisor:	Signature of Chairperson:
--- Dr. Mohammed Moseeur Rahman Assistant professor and Chairperson, Department of ECE East West University, Dhaka, Bangladesh	--- Dr. Mohammed Moseeur Rahman Assistant professor and Chairperson, Department of ECE East West University, Dhaka, Bangladesh

Acknowledgement

At first, we are grateful to almighty Allah for His blessing in successful completion of the task. A special thanks with honor to our supervisor **Dr. Mohammed Moseeur Rahman** for giving us his valuable time, guidance, motivation and encouragement which lead us to the success.

We are so pleased to all of our faculty members of ECE department for their encouragement and support in completion our of Bachelor degree. We also thankful to our seniors and friends who helped us in compilation of this thesis.

A special thanks to our parents whose encouragement and prayer are always with us.

Thank you all for supporting us continuously.

Approval

This thesis on **Silicon Slot Waveguide Based Optical Sensor** by Arifur Rahman, ID: 2014-1-55-008, Md. Abdul Momin, ID: 2015-3-55-012, and Md. Tuhin Sardar, ID: 2015-3-55-015 students of department of Electronics and Communications Engineering, East West University, is submitted for partial fulfillment of the requirements for the degree of B.Sc in Electronic and Telecommunication Engineering and being approved as to its style and contents.

Approved by:

Dr. Mohammed Moseeur Rahman

Assistant professor and Chairperson,

Department of ECE,

East West University.

Abstract

This bachelor thesis explores basically the use of silicon slot waveguide in optical sensing area. Now a day Silicon Slot waveguides are highly used as optical sensor, this sensor are getting more and more interesting and important part of our life. This importance encouraged us to study and work with the Si-slot waveguide optical sensors. In winter season country people most of the time keep the window and door closed. Which increase the CO_2 level in their house and it causes sometimes children's death. If we detect the CO_2 level by using optical sensor then we can reduce children's death. Prawn cultivate gives our country huge remittance. Salinity level maintain important challenge for our prawn pond. If salinity level increases in our prawn pond then we face complication and losses. So we need to control salinity level in our prawn pond. We can control salinity level by using optical sensors. We used Si-slot waveguide optical sensors to detect presence of CO_2 in air, CH_4 in air, to detect level of salinity in sea water and also detecting molecule in medical test sector. In this thesis we have simulated and analyzed fundamental mode of silicon slot waveguide using Comsole Multiphysics simulation software. We also discussed about Finite Element Method (FEM) and given literature review on mostly related to our topic. Also, here we studied different types of slot waveguide based sensors and conducted and present the simulations by using Si slots over silica substrate. These simulation were performed mainly to detect the presence of CO2 and (Methane) in air and concentration of salinity and the results are discussed thoroughly.

Table of Contents: Page

List of Figures

List of Tables:

Thesis Title

SILICON SLOT WAVEGUIDE BASED OPTICAL SEENSOR

Chapter 1

Introduction

1.1 Optical photonics :

Photonics is that the physics of photon generation, detection, and manipulation through emission, transmission, modulation of optical signals and optical signal processing, switching, amplification and sensing. Though the full spectrum covering all light's technical application, most photonic applications are vary within the visible and near-infrared light. The term photonics developed to associate outgrowth of the primary sensible semiconductor light-weight emitters within the early sixties and optical fibers developed in the nineteen-seventies. Photonics as a field started in 1960 with the invention of the optical laser. Other developments are: the laser diode in 1970s, using optical fiber for transmitting information and erbium-doped fiber amplifier. This inventions created the base for the telecommunication revolution of the late twenty century and provided the infrastructure for the net. Applications of photonics are encyclopedic. Photonics covered our all areas from standard of living, for example: light detection, telecommunications, photonic computing, holography, metrology, lighting, information processing, spectroscopy, medicine (health monitoring, vision correction, endoscopy, and surgery), military technology, diagnostics and robotics. [1]

Figure 1.1: Digital Photonics [2]

1.2 Types of optics:

There are two types of optics

1.2.1 Classical optics: In long time ago classical optics invention that light is quantized, when the photoelectric effect is famously narrated by Albert Einstein in 1905.Optics tools embody the refracting lens, the reflective mirror, and varied optical elements and instruments developed throughout the fifteenth to nineteenth centuries. The principle of classical optics such as Huygens Principle developed in the 17th century. Maxwell's equation and wave equations are developed in the 17th century, it's do not depend on quantum properties of light. [1]

1.2.2 Modern optics: Photonics is said to quantum optics, opt-mechanics, electro-optics, optoelectronics and quantum physics. Even, every space has slightly totally different connotations by scientific and government communities and within the marketplace. Quantum optics typically relates elementary analysis, whereas photonics is employed to relate applied analysis and development. [1]

1.3 The term which is mostly related to the photonics:

- The particle properties of light,
- we can using photons to create the potential of signal processing device technologies,
- The practical uses of optics and similarity to electronics.

Optoelectronics connects devices or circuits that related to electrical and optical functions, example: a thin-film semiconductor device. The term electro-optics came into earlier use and specifically encompasses nonlinear electrical-optical interactions applied, example, bulk crystal modulators like the Pockels cell, however additionally includes advanced imaging sensors [1]

1.4 Applications of Photonics: Applications of photonics are everywhere. Enclosed are all areas from the way of life to the foremost advanced science. Few important examples are,

- **Telecom:** Optical fiber communications, optical down convertor to microwave
- **Construction Area:** Laser labeling, label discover, good architecture.

- **Aeronautics:** Photonics using in aviation's to monitor and maintance which is not possible by using normal copper wire.
- **Army:** Infrared sensors, command and management, navigation, search and rescue, mine setup and detection
- **Entertainment:** beam effects, holographic arts.
- **Information processing:** use for encoding, manipulating, storing and decoding information.
- **Dimension:** Frequency and time measurement for finding the location.
- **Photonic computing:** clock distribution and communication between computers, computer circuit boards.
- **Customer equipment:** Bar code, QR scan, laser printer, CD, DVD, remote control device.
- **Medical:** Laser surgery, eyesight correction, tattoo elimination.

1.5: Optical Fiber Sensors

The optical fiber sensors also called as fiber optic sensors are created by using optical fiber or sensing element. These sensors we used to measure some quantities like temperature, vibrations, pressure, displacements, rotations or concentration of chemical species. Optical fiber have so many uses in remote sensing field because does not need any electrical power at the remote location and they also have small size. Optical fiber sensors are extremely suitable for insensitive conditions, high vibration, including noise and extreme heat, wet and unstable environments. For smaller size these sensors can easily fit in small areas and also it can be take it position perfectly in whatever place are needed flexible fiber. We can be calculate wavelength shift by using an optical frequency-domain reflectometry. Optical fiber time-delay can be determine by using a device like as an optical time-domain Reflectometer. [3]

Optical fiber sensors are also secure to electromagnetic interference and do not generate electricity. So they can be used to wherever burnable material or high voltage element electricity as like Jet-Plane Fuel. Optical fiber sensors can be designed to tolerate high temperature as well. [4]

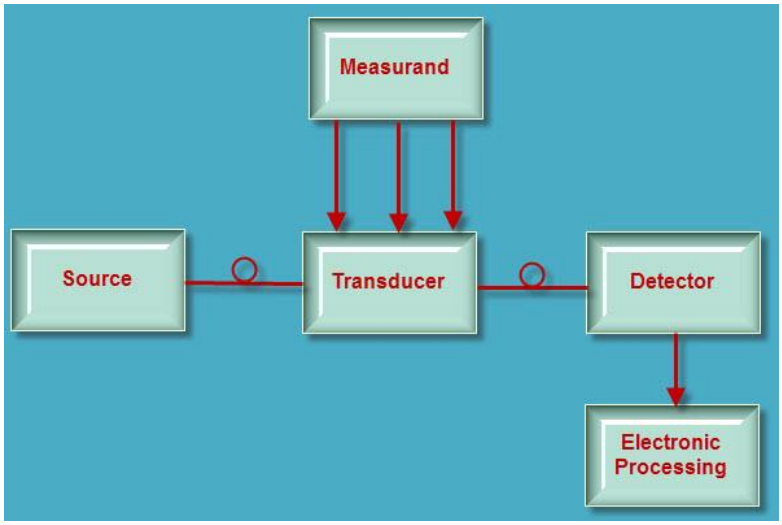

Figure 1.2: Block Diagram of an Optical Fiber Sensor [3]

The basic block diagram of an optical fiber sensor is shown in figure: 1.2. Like any other communication technologies optical fiber sensors comprise of three sub systems like optical source, optical fiber, sensing element, optical detector and end processing devices.

1.5.1 Optical Source: Optical source have Light Emitting diode (LED), Laser and Laser Diode. Light emitting diode and laser diode are mostly used in optical sources for generating the light pulse. Light emitting diode are electronic semiconductor device that can allow pass the current only one direction. Likely, light-emitting diodes are semiconductor devices that emit visible radiation once an electrical current pass through it during a forward direction. When various Light Emitting Diode (LED) placed side by side then they generate pictures. Most of the time Light Emitting Diode (LED), light may be create same color for their single wavelength. This color are red, blue-violet for having wavelength range 700 to 400 nm.

Laser diode is commonly used with its Injection Laser Diode version. Laser diode is also semiconductor devices which produce coherent radiation in the visible or IR spectrum when light passes through it. Laser diodes are widely uses in optical fiber communication as like, CD players, laser printers, remote controls etc. [5]

1.5.2 Optical fiber: An optical fiber is an elastic transparent fiber by drawing slightly thicker glass (silica) or plastic than a human hair. An optical fiber is a very pure, flexible, transparent glass strand that acts as a light pipe for transmitting light between two fiber ends. [6]

1.5.3 Sensing Element: Optical fiber sensing element consists of transducer and measured. A transducer is a device that uses to convert for one signal to another. Sensors have a transducer that receives and responds to a signal. It produces a signal that carries information about the systems. We can used this information by using some kind of telemetry, information or control system. [7] Here measured is use for optical signal measurements.

1.5.4 Optical detector: Optical detector converts incoming optical signal into electrical signals. Two main optical detectors are photon detectors and thermal detectors. Photon detectors are produces one electron with respect to one incoming photon of optical energy. Then the electron is detected by electronic circuity. [8]

1.5.5 End processing Devices: End Processing device used for analyzing optical spectrum. Optical spectrum is given by optical detector. Oscilloscope is an important end device which is used to display and analyze the waveform of electronic signals. A normal oscillator can display AC or DC current which have low signal 1 Hz and high signal a few GHz. But high-end oscillator can display up-to few hundred GHz. [9]

1.6 Types of Optical Fiber Sensors:

Optical fiber sensors can be many types, but depend on application these are three types like as

- Chemical Sensors
- Physical Sensors
- Bio Medical sensors

1.6.1: Chemical Sensors: A chemical sensors is a device that transform chemical information into measurable physical signal that's related to the concentration of a precise chemical species. An analyzer have important component which is the chemical sensors and it may include some devices that is work for signal processing, sampling and data processing. An analyzer is the most important part of the automatic control system. The analyzer working as a monitor with respect to a sampling plan is the function of time acts. The chemical sensors have two functional units one is repeater, and another is a transducer. Chemical information transmitted into an energy in the repeater part and that is measured by the transducer. The chemical information is reworked into associate degree analytical signal and that signal does not show any sensitivity. [3]

1.6.2 Physical sensors: A physical sensors could be a device that's created in keeping with the physical impact and nature. These sensors give us the information about physical property of the system. These types of sensors are in most cases represented by sensors like as photoelectric sensors, piezoelectric sensors, semiconductor piezo sensors and metal strain sensors. [3]

1.6.3 Bio Medical Sensors: Biomedical sensors provide us the significant combination between biological environmental an electronic system, covered by though condition of high compatibility with the hosting setting, light-weight, high responsibility, long-expected period of time, and attractiveness. These types are sensors are unique. [11] These sensors are used to transmit non-electrical portion in biomedical fields into easily measurable electrical portion. For this sense, these kinds of sensors are entered in health care inquiry. This sensing method is the most important key to assembling human pathological and physiological report. [3]

1.7 Working principle of Optical fiber sensors:

Optical fiber sensors work supported the principle that lightweight from an optical device or Any super luminescent supply is transmitted via glass fiber, experiences changes in its parameters either within the glass fiber or fiber Braxton Bragg gratings and reach a detector that measures these changes. Optical fiber sensors have an optical fiber cable which is connected by an amplifier or a remote-control sensor. The fiber optic cable consists of a glass or plastic core encircled by a layered product of protection material. The distinction in densities between the core and the layer allows the cables to act supported the whole internal reflection principle, that states that the sunshine putting a boundary between 2 parts are completely mirrored with none loss in light energy. The mirrored light is then transmitted to a sensor/detector that converts the sunshine energy into an electrical signal [10]

1.8 Application of Optical Fiber Sensors:

Optical fiber sensors are used in various types of application like as

- Analysis of physical properties like temperature, displacement, velocity, strain in structures of any size or any form.
- Observe the physical condition in real life.
- Houses and overpass, underpass, bunk, custom architecture.

- Night vision camera, electronic security systems, Partial discharge detection and activity wheel numerous vehicles.

Here, we have been discussed about an over view and application of an optical fiber sensors. Here we seen using optical fiber sensors there are lots of benefits for large distance communication that cover small size, high sensitivity, light in weight, high bandwidth and mobilization. All these characteristics build the most effective use of fiber optic as a sensing element. [3]

In chapter 1 we discussed about introduction of optical sensors, here we included optical photonics, optical fiber sensors and its application. In chapter 2 we given an overview about some papers or journals which is related to our topic. Then we briefly explained FEM in chapter 3. Next, we reviewed Comsole user guide line in chapter 4. Results and simulation part, we discussed in chapter 5. And finally, we given a conclusion and about future work in chapter 6.

Chapter 2

Literature review

Carlos Angulo Barrios had given an overview of optical slot waveguide based biochemical sensors. In this paper Carlos Angulo Barrios had been presented about integrated optics; slot-waveguides; optical sensors; biosensors and also told about recent progress in slot waveguide based biochemical sensors like slot-waveguide based refractometric sensors, slot waveguide microring resonators, labeling-based optical bio-sensing, an opt-mechanical transducer for slot-waveguide based biochemical sensors. A brief survey of the fundamentals of slot-waveguides based optical sensors had been presented in this paper. A Slot-waveguides is an optical waveguide that allows light to be guided and strongly confined inside a nanometer-scale region of low refractive index region by total internal reflection (TIR). Thus, stronger light-analytic interaction may be obtained as compared to it realizable by a traditional waveguide, during which the propagating beam is confined to the high-refractive-index core of the waveguide. In addition, slot-waveguides are fictional by using CMOS compatible materials and technology, facultative miniaturization, integration with electronic, photonic and fluidic elements in a very chip, and fabrication. These benefits had created the employment of slot waveguides for sensitive organic chemistry optical integrated sensors associate rising field. [11]

In this article, they used slot waveguides rising field for sensitive organic chemistry sensing. Hitherto, fluid Little Rhody state detection, label-free and labeling-based bio-sensing, trappings and transport of nanoparticles which including biomolecules and opt-mechanical transduction-based bio-detection are either incontestable or in theory analyzed by exploitation CMOS-compatible material systems: Si3N4/SiO2 and Si/SiO2. Moderate index-contrast Si3N4/SiO2 is a smaller amount capable to device structural defects and permits wider slot-widths merely liquid and particle incoming within the slot region; high index-contrast Si/SiO2 offers U.S.A. higher E-field increase the slot, for that reason higher sensitivity and potential larger integration level. In all condition, slot-waveguide has been more useful if we compare it with other conventional waveguides in terms of sensitivity and potential use in applications which require the fusion of Nano-photonics and Nano-fluidics. Future work is expected to be

focused on the extension to other material systems for improvement of sensing and improvement of advanced sensors architecture based on slot-waveguide for practical in real-life implementation [11]

Francesco Dell'Olio and Vittorio M. N. Passaro had given an overview of Optical sensing by optimized silicon slot waveguides. In this paper, Francesco Dell'Olio and Vittorio M. N. Passaro had been presented a theoretical investigation of silicon-on-insulator milli-micron slot waveguides for strongly sensitive and compact chemical and organic chemistry integrated optical sensing is planned. Slot guiding structures facultative high optical confinement during a low refractive index very tiny region are incontestable to be very sensitive to either cowl medium index of refraction amendment or deposited receptor layer thickness increase. Modal and confinement properties of slot waveguides had been researched, discussed the influence of fabrication tolerances. The sensitivity of slot waveguide had been computed and compared with that manifested by other silicon nanometer guiding characteristics like rib or wire waveguides or with experimental literature values.[12]

In this paper, they had carried out a detailed inquiry of modal properties and the performance of silicon slot guiding properties. Optical technologies play a central role in chemical and organic chemistry analysis and their employment in lab-on-a-chip microsystems has been incontestable as terribly engaging. In this scheme, optical chemical sensing has been reaching noticeable attention by using guided waveguide devices. Measurement sensitivity depends on optical field distribution within the cowl medium, thus one amongst the foremost necessary style tasks is that the conductor improvement so as to maximize its sensitivity. Silicon technology is superior photonic devices and optical integrated circuits have been incontestable as a really attention-grabbing prospect for a good variety of application fields, as well as sensors. For insistence, Si integrated lab-on-a-chip systems during which photonic sensing functions are integrated with electronic intelligence and wireless communications may be used in environmental observation and medical specialty. Recently, Silicon-on-Insulator (SOI) sub-micrometer chemical element wire waveguides are incontestable terribly engaging for integrated optical sensors, as a result of the exhibit a sensitivity considerably larger than that assured by alternative guiding structures supported chemical element oxy-nitride (SiON), chemical compound materials or chemical element. When 2 Si-wires are terribly about to one another, it's potential to understand another SOI micro millimeter guiding structure, sometimes referred to as SOI slot waveguide. A great vitiation of optical devices has been recently projected or fictional by victimization slot waveguides, together with microring resonators,

optical modulator electrically pumped-up light-emitting devices, directional couplers, all-optical logic gates, and beam splitters. However, a Finite Element Methodology (FEM)-based modal investigation dedicated to learning the influence of slot waveguide geometrical parameters on optical power fraction confined within the low-index gap region has been additionally meted out.

In this paper, they perform detailed about SOI slot waveguide modal investigation, taking into consideration the fabrication tolerance results and also the chance that a skinny Si plate-like layer is placed below the slot structure. They discussed the sensitivity of conventional slot and slot rib waveguide has been measured and developed. They also compared the sensitivity of slot waveguide with other guiding structures like SOI rib and silicon wire. They used always fixed operating wavelength 1550nm. [12]

The implementation of that waveguides has been properly discussed for chemical and biochemical sensing purposes. Conventional slot waveguides are tested to be terribly sensitive to hide medium ratio modification, particularly once a quasi-TE mode is considered. Mistreatment associate degree optimized set of geometrical parameters, a sensitivity surpassing the unity are often obtained. That sensitivity value is larger than other nanometer guiding structures, even highly sensitive, as like Si-wires. Here also studied in silicon slot waveguide SOI rib should be very close to each other. The use of this guiding structure and of standard slot conductor for surface sensing has been mentioned, demonstrating that micro-millimeter SOI rib, Si-wire and slot waveguides (conventional and rib) exhibit similar values of most surface sensitivity. Non-vertical sidewall influence on slot guiding structures has been investigated in terms of effective index, refraction and sensitivity, with the result that typical slot waveguides are additionally influenced than slot rib waveguides by this fabrication tolerance. Because the sensitivity of integrated optical sensors strongly depends on their guiding structure, the results presented in this paper can be used as design criteria. In addition, they are very important for indicative that micro-millimeter SOI slot waveguides can be utilized to fabricate exceed sensitivity and ultra-compact integrated optical chemical or organic chemistry sensors supported varied architectures, like Mach-Zehnder measuring device, directional mechanical device or microring resonator. [12]

Kristinn B. Gylfason KTH Micro and Nano-systems had given an overview of bio-sensing with silicon photonics. In this article, they discussed importance of bio-sensors, definitions of bio-sensors, photonics waveguide-based bio-sensors fundamental, silicon waveguide as a bio-

sensors, liquid sample handling by bio-sensors and reducing sensitivity of temperature. Here they also explain strip waveguide and a lot of waveguides. In both cases, they used wavelength factor 1310 nm. From this paper, we know that silicon slot waveguide had two advantages for a high refractive index. One advantage is ring can be made very small by using bending loss without reducing quality factor and another is silicon surface evanescent electric field is very high for having high sensitivity in surface sensitivity.[13]

Souvik Ghosh and B. M. A. Rahman had given an overview of an Innovative Straight Resonator Incorporating a Vertical Slot as an Efficient Bio-Chemical Sensor. In this paper, they also discussed the Finite Element Method (FEM), Integrated Optics, Resonator, and sensors. They discussed a compact and integrated label-free refractometric biochemical sensing element supported silicon-on-insulator (SOI) is planned and mostly considered at the telecommunication wavelength of λ = 1550 $\boldsymbol{nm}$. This device incorporated a 3-dimensional Fabry-Perot cavity within the nano-scale regime with the most footprint space around 470 × 473 $\boldsymbol{nm}$2. A resonance shifts of 5.2 $\boldsymbol{nm}$ is according to associate ultra-thin bio-layer sensing. Besides, associate improved most sensitivity is additionally achieved for the bulk index of refraction amendment in surroundings. As a chemical device, an awfully low detection limit can also be attainable to attain by this device. All the numerical investigations and optimizations were allotted within the frequency domain by a numerically economical and rigorous full vectorial H-field based mostly 2nd and 3D Finite component strategies. A 3D-FEM code is developed and wont to resolve the wavelength dependencies of the resonator. Chance of simple CMOS fabrication and integration opportunities build this structure as a prospective and economical lab-on-chip device. [14]

In this paper, they report a SOI-based, single vertically-slotted resonator as associate degree economical organic chemistry detector, which is able to be simple to fabricate. Device performance has been studied for surface sensing with a five nm bio-ad layer and bulk index of refraction changes within the cowl and slot region. A rigorous full vectorial 3D-FEM is developed and accustomed to simulating the device for various sensing applications. They acquire a record sensitivity of 5.2 nm resonance wavelength shift for surface sensing. On the other site, associate degree improved linear ringing wavelength shift of 635 nm/RIU and 820 nm/RIU are achieved for unvaried refractometric sensing. The detection limit as low as 6.1 × 10−6 RIU is often achieved. Typical waveguide loss for vertical slots has been measured as &lt less than twenty dB/cm. After all, water additionally absorbs lightweight at 1550 nm and this worth has been given as 47.5 dB/cm. In their style, nearly two-hundredth of the ability is

confined within the water face. Thus, for the vertical slotted resonator shorter than 1 μm, as reportable here, the propagation loss of the slotted structure is going to be terribly tiny and neglected in our simulations. A rigorous least-squares boundary residual (LSBR) technique is employed to calculate the facility transfer, the rear reflection constant (ρr) and transmission loss of the butt coupled strip waveguide and slotted resonator for various gaps. For 3 totally different gaps 250, 300 and 400nm, the facility transfers from strip to fit resonator are 1.67%, 1.12%, and 0.512%, severally. Some input signals additionally mirrored from the junction between the input guide and therefore the resonator section with slot guide and these reflection coefficients (ρr) are calculated as 0.024, 0.020 and 0.012, for separations 250 nm, 300 nm, and 400 nm, severally. On the opposite hand, the coupling losses at this junction also are calculated by victimization the LSBR technique. These coupling losses are zero.2886 dB, 0.1956 decibels and zero.0833 decibel for separations 250 nm, 300 nm, and four hundred nm, severally. It may be noted that the 250 nm gap provides higher temporary coupling to fit waveguides however with additionally higher butt-coupling loss from the input guide, whereas the four hundred nm gap provides less temporary coupling however with better butt-coupling potency.So an acceptable separation might be vary of 250 to 400 nm, individually.[14]

Their proposal serves the winning demonstration of label-free organic chemistry sensing applications of the low-index confined magnetism field in an exceedingly slotted Fabry-Perot resonant structure by employing a full-vectorial 3D-FEM method. This Nano structural pure mathematics is comparatively easy and compact compared to different complicated photonic devices like slotted ring resonator and Nano-Bragg grating sensors. This may be realized in observe with the assistance of well-matured progressive fabrication technologies and surface chemistry. Supported the preliminary results this slot resonator device shows an excellent potential to use as an organic chemistry detector.[14]

Ghosh, S. and Rahman, B. M. had given an overview about evolution of Plasmonic Modes in a Metal Nano-Wire Studied by a Modified Finite Element Method(FEM). In this paper, they reviewed Computational electromagnetic methods, Finite element method, Surface Plasmon, Plasmonics, and Waveguides. A finite dimension fragile metal film plasmonic nanowire with its distinctive feature of sub-wavelength light-weight guiding is finding several applications in compact integrated Nano-photonic circuits and sensors. The full-vectorial finite part technique is turning into a crucial simulation tool for the analyses of such exotic waveguides. Rather than a penalty approach reported earlier, an additional direct divergence formulation considering every discretized element's optical properties to eliminate non-physical modal eigenvectors

has been exploited and is reported here. Long and short-range basic and higher-order plasmonic modes and supermodes of a pure metal nanowire and their evolutions with conductor pure mathematics, close identical and non-identical insulator protective cover materials and in operation wavelength are totally studied. Fascinating long-range modal properties like, supermode formation, complicated section matching, and mode evolution in identical and non-identical clad metal nanowires are ascertained and explained well together with supermode profiles. This study is anticipated to assist in understanding the evolution of plasmonic guided modes in compact active and passive integrated photonic devices containing metal slender strips. [14]

For this study, they need to be changed their previous penalty approach to contemplate waveguides that contain each positive and negative stuff constant, to eliminate the spurious modes additional expeditiously within the characterizations of plasmonic modes. A detail modal investigation has been applied to check the Nano plasmonic modal behavior of guided modes supported by an easy metal film embedded into insulator background materials. Plasmonic modes have higher effective indices than the encircling protective covering ratio. As they approach cut-off, the mode fields unfold into protective covering region and plasmonic modes evolve into background quasi-TEM mode that ends up in a discount in mode propagation loss. Depending on totally different light-guiding conditions long and short area plasmonic elementary and higher-order modes are studied. Thus, the numerically investigated delimited SPP modal analyses of an easy silver nanowire with success demonstrate the utility of our planned divergence changed FV-FEM. Besides, these enticing Nano plasmonic modal natures with completely different light-guiding conditions provide intuitive concepts within the style and fabrication of complicated plasmonic devices, like logic gates, switch, BUS router, modulator, and nanowire optical device. An acceptable choice of background material materials and metal nanowire style parameters may lead to regulate of the long-range subwavelength confined plasmonic modes and their incorporation in compact integrated plasmonic and hybrid plasmonic active and passive nanophotonic circuits polarization dominant devices nonlinear and sensing applications.[14]

Yuhei Ishizaka, Shuntaro Makino Takeshi Fujisawa, KunimasaSaitoh they presented a metal-assisted silicon Slot Waveguide for highly sensitive gas detection. In this paper, they proposed to highly sensitive gas detection by using metal assisted silicon slot waveguide.[15]

In this paper, they are using Slot waveguides, surface Plasmon polarization, and finite element methods. To show the prevalence of the projected structure, the optical confinement thinks about the gas region and therefore the sensitivity are in theory, investigated exploitation of the 2-D vector finite element methodology. Analytical results show that the planned structure are able to do a heavy light-weight confinement within the gas region with respect to the standard slot waveguide. The maximum optical confinement issue of 85 is obtained within the planned structure, which is just about 2.5 times larger than the traditional slot conductor. To boot, results show that the planned structure includes a massive sensitivity compared with the traditional slot waveguide. Finally, they proposed a ring resonator-based structure is considered to evaluate the quality factor and to extend the legality of outcome collect by 2-D simulation. They have recommended getting substantial light confinement in the low refractive index region for highly sensitive gas detection by using a metal-assisted silicon slot waveguide. And also, the results show that the projected structure encompasses a huge sensitivity compared with the traditional slot waveguide. Additionally, to the current, we tend to clarify that the mode coupling that deteriorates the sensitivity happens between the TE mode and therefore the TM mode at specific structures. To neglect this, parameters that have an outsized union magnitude relation mustn't be elect once constructing Rhode Island sensors. Finally, they analyze a hoop resonator supported the planned structure mistreatment of the 3-D VFEM for the cavity drawback to judge the standard issue. They get quality factor approximately 4600 by using 3-D simulation. From the outcome of the sense figure out by 3-D analysis, it's decisive that estimating the sensitivity from the optical confinement issue is sufficiently helpful for the planned structure with the metal layer. The prospective field of study adds the describe style of cavities and empirical verification of the benefits of our structure for the implementation of a sensitive gas detector.[15]

Tom Claes, Jordi Girone`sMolera, Katrien De Vos, Etienne Schacht, RoelBaets, and Peter Bienstman had given and overview about Label-Free Biosensing with a Slot-Waveguide-Based Ring Resonator in Silicon on Insulator. In this paper they review Biosensor, ring resonator, silicon on insulator, slot waveguide. Experiments show that its 298 nm/RIU sensitivity and a detection limit of 4:2*10^5 RIU for changes within the index of refraction of the highest protective cover. we tend to prove for the primary time that surface chemistry for selective label-free sensing of proteins are often applied within a 100 nm-wide slot region associate degreed demonstrate that the applying of a slot conductor rather than a traditional waveguide

will increase the sensitivity of an SOI ring resonator with an element 3.5 for the detection of proteins. Here they tend to see that numerically optimized SOI slot waveguides for label-free bio-sensing of proteins and conferred a slot-waveguide-based ring resonator in SOI with a footprint of solely 13μm*10μm, fancied with optical lithography. Experiments showed 298 nm/RIU sensitivity and a detection limit of 4:2*10^5 RIU for ratio changes of the entire prime facing. [16]

In this paper, they verified for the primary time that surface chemistry for selective label-free sensing of proteins is applied within a one hundred nm wide slot region Associate in Nursing incontestable that the applying of a slot conductor rather than a traditional waveguide will increase the sensitivity of an SOI ring resonator with an element three.5 for the detection of proteins. Finally, they tend to plan any enhancements of the detector for Associate in nursing improvement of the detection limit. Here they tend to see that numerically optimized SOI slot waveguides for label-free bio sensing of proteins and conferred a slot-waveguide-based ring resonator in SOI with a footprint of solely 13 μm*10 μm, visualize with optical lithography. In this Experiment showed 298 nm/RIU sensitivity and a detection limit of 4:2*10^5 RIU for ratio changes of the whole prime facing. They verified for the immediate time that surface chemistry for selective label-free sensing of proteins is applied at intervals a 100nm wide slot region generate in Nursing incontestable that the applying of a slot conductor instead of a conventional conductor can increase the sensitivity of an SOI ring resonator with a part that has 3.5 for the detection of macromolecule. Finally, they get to plan any improvement of the detector for generate in the nursing improvement of the detection limit.[16]

Y. Tomono, H. Hoshi, and H. Shimizu had given an overview about CO2 Detection with Si Slot Waveguide Ring Resonators Toward On-chip Specific Gas Sensing. They made-up a Si slot conductor ring resonator detective work CO2 gas with Refractive index distinction of 1.5x10-4 and sensitivity of 3x102 nm/RIU. The device satisfies every detecting capability and compatibility with bio-layer toward on-chip specific gas sensing. [17]

They designed Si slot waveguide sensors considering the overlap of bio-layer with lightweight propagation section so as to comprehend specific gas detection with higher sensitivity. The unreal Si slot waveguide ring resonators detected CO2 with Refractive Index distinction of 1.5x10-4 and sensitivity of 3x10^2 nm/RIU, which means that the device satisfies detection capability and compatibility with bio-layer toward specific gas sensing. [17]

Chao Pan and B. M. A. Rahman presented High-Sensitivity Polarization-Independent Biochemical Sensor Based on Silicon-on-Insulator Cross-Slot Waveguide. In this paper they used some important terms like as, Biochemical sensing, cross-slot waveguide, finite element analysis, high sensitivity, polarization independent, silicon photonics. Slot waveguides reportable therefore fare powerfully polarization dependent. The conception of a completely unique cross-slot waveguide is bestowed here, which contains each vertical and horizontal slot and supports the ability sweetening within the slot region for both the quasi-TE and quasi-TM polarizations. This Waveguide may be invented by exploiting well-developed CMOS technology. For the unpolarized in operation lightweight, the cross-slot waveguide is optimized to own the most total slot confinement factors for the 2 polarizations. As for a polarization-independent style, confinement within the slot for every polarization will reach 39.4% once the semiconducting material core dimension and height are set to around 223 and 216 nm, severally. They are shown here that an organic chemistry detector using cross-slot-WG exhibits significantly higher sensitivity, compared to either a vertical-slot WG or a horizontal-slot-WG-based organic chemistry detector. As AN example, once each the vertical slot breadth and horizontal slot height are set to a 100 nm, its sensitivity is sort of double compared with an easy vertical or horizontal slot with a 100 nm gap. [18]

A correct full-vectorial field based mostly FEM is employed to check the characteristics of the organic chemistry sensors supported the SOI vertical, horizontal, and a unique cross-slot that consists of each vertical and horizontal slots. For the quasi-TE polarization, the slot confinement issue of the cross-slot waveguide is as high as that of the vertical slot Waveguide with identical waveguide height. Similarly, for the quasi-TM polarization, the slot confinement issue of cross-slot Waveguide is additionally as high as that of the horizontal slot waveguide with an identical waveguide dimension. It's true that the cross-slot waveguide will take blessings of each the vertical and horizontal slot waveguides and support the field improvement within the slot region for each the quasi-TE and quasi-TM polarizations and such a structure is simply fancied by exploitation customary CMOS technologies. For non-contradictory operational light-weight, the cross-slot waveguide is developed to possess the most addition of the slot confinement factors for the two polarizations, whose values are concerning up to the addition of the slot confinement factors of the quasi-TE mode within the vertical slot Waveguide with constant waveguide height that of the quasi-TM mode among the horizontal slot conductor with a similar waveguide width. A polarization-independent style of the organic chemistry device is conjointly achieved supported by the cross-slot conductor successfully.

When the semiconductor core breadth and height are set to around 223 and 216nm, severally, the slot confinement issue for every polarization canreach39.4%, nearly identical as that for the quasi-TE mode within the vertical slot waveguide with the same waveguide height and additionally that for the quasi-TM mode in the horizontal slot waveguide with the same waveguide width. Here they determined and related the biochemical sensitivity based on the three types of waveguides and also find out cross-slot waveguide had better performance for sensors. When the vertical slot width and horizontal slot height are same, and the value is 100nm then cross-slot waveguide gives us double sensitivity rather than vertical slot and horizontal waveguide. [18]

A slot waveguide is an optical waveguide that guides strongly confined light in a sub wavelength scale low refractive index region by total internal reflection. A slot-waveguide consists of 2 strips or slabs of high-refractive-index (nH) materials separated by a subwavelength-scale low-refractive-index (nS) slot region and enclosed by low-refractive-index (nC) protective covering materials.

The principle of operation of a slot-waveguide is predicated on the separation of the electrical field (E-field) at high-refractive-index-contrast interfaces. Maxwell's equations state that, to satisfy the continuity of the conventional element of the electrical displacement field D at Associate in nursing interface, the corresponding E-field should endure a separation with higher amplitude within the low-refractive-index aspect. That is, at Associate in Nursing interface between 2 regions of stuff constants εS and εH, respectively:

$$D_S^N = D_H^N$$

$$\varepsilon_S E_S^N = \varepsilon_H E_H^N$$

$$n_S^2 E_S^N = n_H^2 E_H^N$$

Where the superscript N indicates the normal components of **D** and **E** vector fields. Thus, if $n_S << n_H$, then $E_S^N >> E_H^N$.

Given that the slot vital dimension (distance between the high-index slabs or strips) is such as the decline length of the elemental Eigen mode of the guided-wave structure, the ensuing E-field traditional to the high-index-contrast interfaces is increased within the slot and remains high across it. The facility density within the slot is way more than that in the high-index

regions. Since wave propagation is because of total internal reflection, there's no interference result concerned and also the slot-structure exhibits terribly low wavelength sensitivity.

In this article, they had presented principle of slot waveguide, operation, fabrication and application of slot waveguide.The slot-waveguide was born in 2003 as sudden outcome of theoretical studies on metal-oxide-semiconductor (MOS) electro-optic modulation in high-confinement semiconductor photonic waveguides by Vilsonrosid dicot genus de Almeida and Glen Gebhard Angulo Barrios, then a Ph.D. student and a Postdoctoral Associate, severally, at university. Theoretical analysis and experimental demonstration of the primary slot-waveguide enforced within the Si/SiO2 material system at 1.55μm operation wavelength were reportable by Cornell researchers in 2004. Since these pioneering works, many guided-wave configurations supported the slot-waveguide conception are projected and incontestable. Recently than 100% if optimized properly, and thus the effective power coupling length between the waveguides can significantly be reduced, in 2016, it is shown that slots in a pair of waveguides if off-shifted away from each other can enhance the coupling coefficient even more. Planar slot-waveguides are made-up in several material systems like Si/SiO2 and Si3N4/SiO2. Each vertical (slot plane is traditional to the substrate plane) and horizontal (slot plane is parallel to the substrate plane) configurations are enforced by exploitation typical micro- and nano-fabrication techniques. These process tools embrace beam lithography, lithography, chemical vapor deposition, reactive-ion etching and targeted particle beam.[19]

A slot-waveguide produces high E-field amplitude, optical power and optical intensity in low refractive index materials at levels that cannot be achieved with conventional waveguides.
This property permits extremely economical interaction between fields and active materials, which can result in all-optical change, optical amplification and optical detection on integrated photonics. Sturdy E-field confinement may be localized in an exceedingly nanometer-scale low-index region. As initial identified in, the slot wave guide may be wont to greatly increase the sensitivity of compact optical sensing devices. [19]

Chapter 3

Finite Element Method

3.1 Introduction:

The basics of the nodal finite element method (FEM)are discussed in this section, including the element of the first order and the element of the second order. The FEM nodal is introduced for the scalar definition of the 2D waveguide cross-section propagation constant. It is then expanded to include the study of the time domain under perfectly matched layer which absorbs boundary conditions. A basic optical grating-based sensor is then modeled using the FEM time domain. In addition, the total vector analysis is addressed by applying the penalty function approach to the nodal FEM and the method of the vector finite element (VFEM). A global weighting factor is used for the penalty function model to integrate the effect of the divergence-free equation. In the VFEM, nodes are used to represent the field's orthogonal component while the edges are used to represent the tangential component to correctly apply the boundary conditions. In the finite element method (FEM),the corresponding functions to which a variation rule is applied where computational domain are separated into so called elements[20-24] .Then an equivalent model of discretization is constructed for each element. After that all element contributions in the analysis region are assembled. The FEM can be regarded as a special type of Rayleigh-Ritz method, where piecewise polynomial functions are used for test functions and a finite number of unknowns are used instead of infinite degrees of freedom in the current system. Analytical functions described over the analytical region are used to describe the process in analytical techniques without subdivision. Therefore, these types of methods succeed only in simple geometries. One of the known methods of discretization is the finite difference method FDM. The FDM historically uses regular grids within which the intersection interface is discrete [25, 26]. Unfortunately, regular grids fail to describe curved and irregularly shaped geometries. The explanation behind this is that such nodes cannot be modified to establish the boundary for curved structures at the intersection of grid lines. Therefore, standard grids are not able to model fast variations in the field accurately. On the other hand, the FEM divides the regions of the analysis into components but unlike the FDM these elements will take different forms such as triangles or rectangles for 2D analysis and 3D for tetrahedral analysis. By using these shapes, the FEM allows irregular grids to be used. Therefore, the FEM is more capable of modeling fast variations in the field than FDM. It is also easy to approach to inhomogeneous and anisotropic

materials. In addition, the FEM technique can be established using the Galerkin method, a weighted residual method as well as the variation method. In this section, the discussions are confined to the Galerkin approach only. The rest of the chapter is organized as follows after the introduction, an overview of the method of finite elements is presented. The scalar finite element method is then used for analyzing the optical waveguide mode. After that the FEM is adopted for time domain analysis. The penalty function method and the finite vector component are then discussed for the complete vector analysis of optical wave guides. A photonic biosensor is investigated based on the basis of full vector analysis.

3.2 Finite Element Method Overview

Finite element procedure:

The basic steps for constructing the study of any photonic model using FEM can be described as follows:

1. Discretization of one's value system into many shorter domains of components;
2. To determine unknown parameters, set up the interpolating equation by the values at t he elemental nodes or boundaries. It can be a region or potential;
3. Configuration of the individual equations of discrete components to form solutions of global eigenvalue;
4. Solving global equations with a matrix solver of its own value;
5. Lastly, to obtain desired unspecified variables, postprocessing of the own values and a ssociated eigenvectors.

3.2.1 Setup Element Interpolation:

Once the domain is discrete with the correct components, the component form functions must be interpreted in terms of the unspecified variational parameters. Any continuous function over the computational domain can be approximated using the polynomial interpolation function or form function. The selected function should be continuous within and across element boundaries. The functions are not suitable for variational formulations without continuity and the electromagnetic field or potential cannot be determined by summing up the individual contributions of the elements. The number of terms must be equal to the number of nodes in the element for a special shape function for a specific element. The triangular structure of Pascal gives a good graphical representation of the relationship between the number of

component nodes and the number of terms in the polynomial for a 2D discretization of the domain.

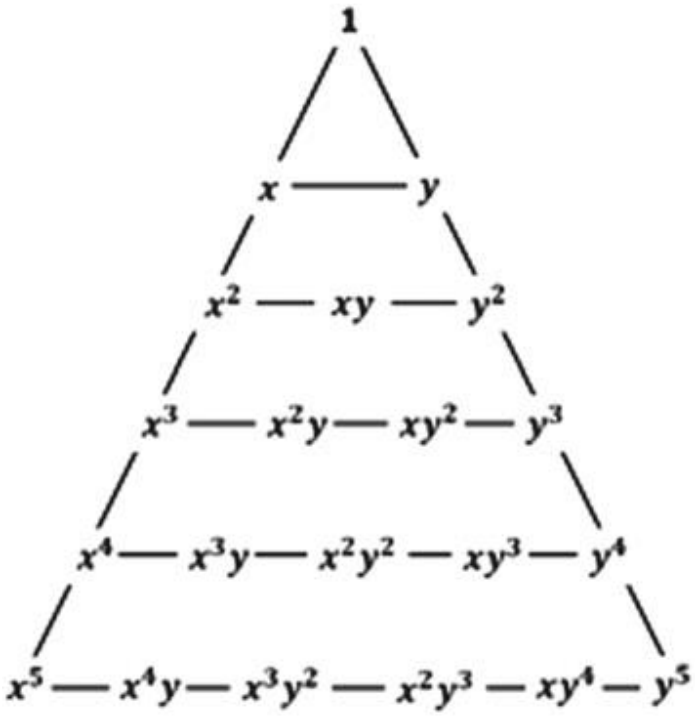

Fig 3.1: Pascal triangle exhibiting the relationship between element nodes number and the number of terms in the shape function (*Ni*) [49]

To construct the shape functions for the elements of different types, we introduce the Lagrange interpolation polynomials (Li). For a linear triangular (2D) element and tetrahedral (3D) element, these Lagrange polynomials, which are also known as the area coordinates, are given by

$L_i = \frac{1}{2Ae} [a_i + b_i x + c_i y]$ for 2D (3.1)

$L_i = \frac{1}{2Ve} [a_i + b_i x + c_i y + d_i z]$ for 3D (3.2)

where A_e and V_e are the area and volume of the 2D triangular and 3D tetrahedral element, respectively. The subscript e denotes the element number. The a_i, b_i, c_i, and d_i are constant coefficients.

If we consider a point Q inside a discretized element, we can get sub-elements from each element (sub-triangles and sub-tetrahedral from triangular and tetrahedral elements, respectively). Now, the area and volume of those sub regions can be expressed as follows:

The area defined by the point Q and nodes 2 and 3 is

$$A=\frac{1}{2}\begin{bmatrix}1 & x & y\\ 1 & x_2 & y_2\\ 1 & x_3 & y_3\end{bmatrix} \quad (3.3)$$

$$=\frac{1}{2}\left[(x_2y_3 - x_3y_2) + (y_2-y_3)x + (y_2-y_3)\right]$$

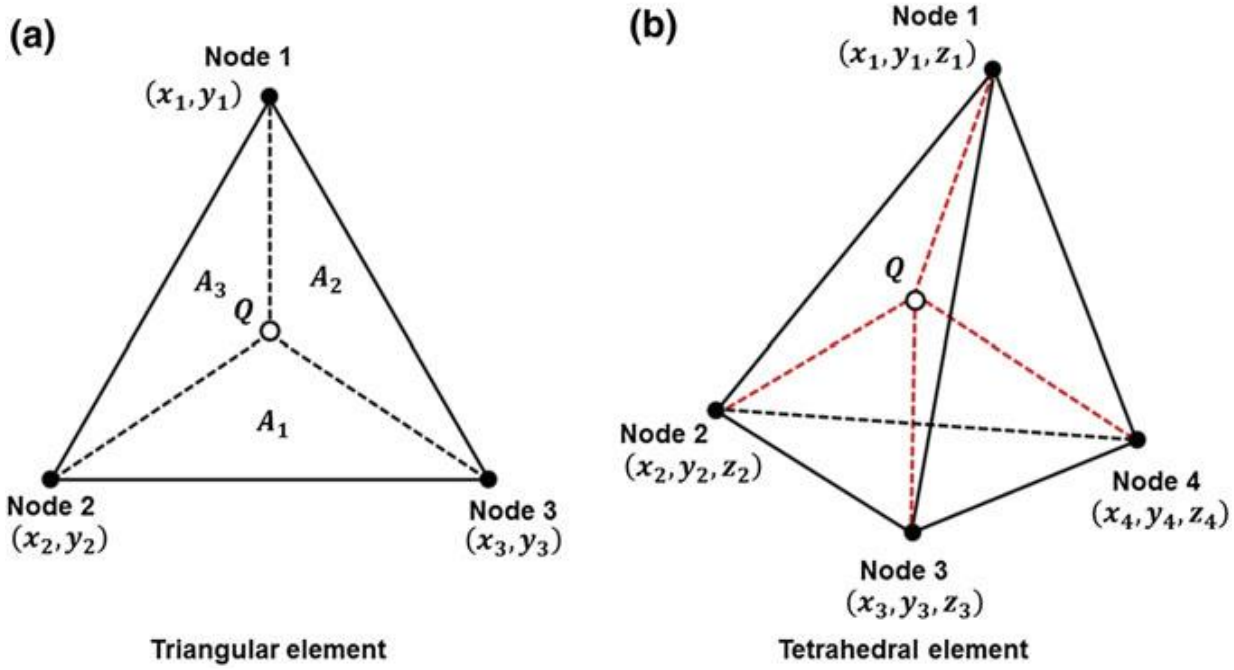

Fig 3.2: **a** Linear triangular elements for 2D discretization and **b** linear tetrahedral elements for 3D discretization. The Q is taken as any point inside the element of arbitrary coordinate (x, y) for 2D and (x, y, z) for 3D [49]

Similarly, the volume defined by the point Q and nodes 2, 3, and 4 is

$$v = \frac{1}{6}\begin{bmatrix}1 & x & y & z\\ 1 & x_2 & y_2 & z_2\\ 1 & x_3 & y_3 & z_3\\ 1 & x_4 & y_4 & z_4\end{bmatrix} \quad (3.4)$$

Reutilizing those constant coefficients a_i, b_i, c_i are for 2D and a_i, b_i, c_i, and d_i for 3D),the L_e^i functions for the all three nodes of a triangular element can be defined as:

$$\begin{bmatrix}L_1\\ L_2\\ L_3\end{bmatrix} = \frac{1}{A^e}\begin{bmatrix}A_1\\ A_2\\ A_3\end{bmatrix}\frac{1}{2A^e}\begin{bmatrix}a_1 & b_1 & c_1\\ a_2 & b_2 & c_2\\ a_3 & b_3 & c_3\end{bmatrix} \quad (3.5)$$

The functions of Lagrange here depend on the selection of point Q in the component. Similarly, the Lagrange functions can be defined in a compact matrix as for a 3D tetrahedral component.

The functions of the Lagrange depend on the elemental area and volume, respectively, for 2D and 3D elements. Such functions are therefore often named as directions of area and volume for 2D and 3D problems.

First, each node of the element (linear and quadratic triangular or tetrahedral) is numbered as shown in Fig to formulate the shape function. 3.3. The node numbers for a 2D element consist of three digits, while it has four digits for a 3D element. The number of digits depends on the number of area or volume coordinates required to define an element (Lagrange functions). For example, triangular 2D and 3D tetrahedral elements need to be defined by three region and four volume coordinates, respectively. Nodes 1, 2, and 3 are numbered as (100), (010), and (001), respectively, of a 2D linear triangular element. Thus, the node-related shape function N_i^e can be expressed as: [26]

$$N_i^e = Q_p^{(n)} L_1 Q_q^{(n)} L_2 Q_r^{(n)} L_3, \; p + q + r = n \qquad (3.6)$$

Where p, q, r denotes the number of the individual nodes and n denotes the order of the element. For example, node 1 values p, q, and r are 1, 0, and 0, respectively. The first multiplied term can be defined as:

$$Qp^{(n)} L_1 = \frac{n}{p!} \prod_{m=0}^{p-1} \left((m+1) L_1 - m \right) \qquad (3.7)$$

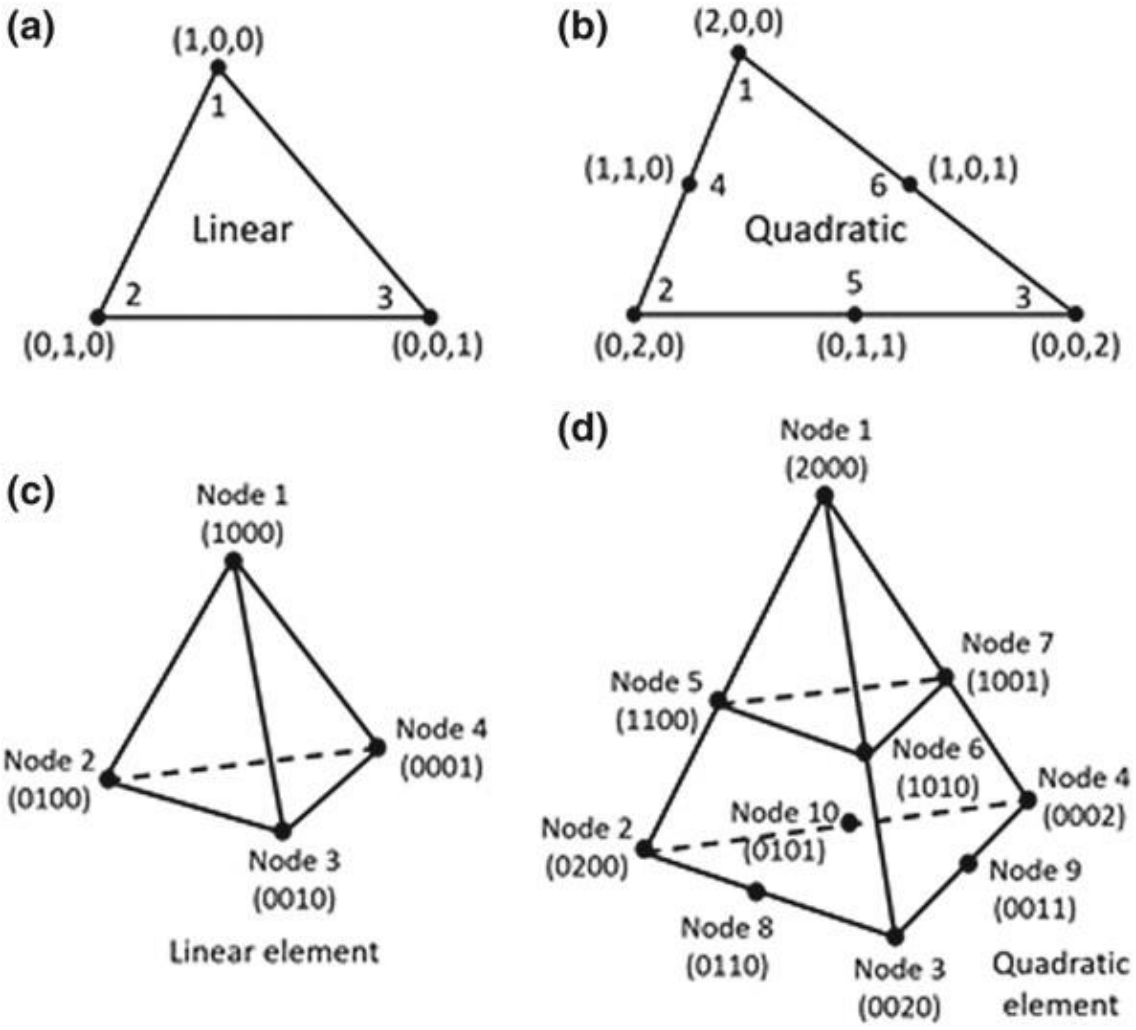

Fig 3.3: Linear and quadratic elements and their node numbering scheme depending on the element order, and **b** are the linear and quadratic 2D triangular elements, respectively. **c** and **d** are the liner and quadratic 3D tetrahedral elements, respectively. [49]

The other multiplied terms, $Q_q^{(n)}L_2$and $Q_r^{(n)}L_3$, are defined as [27], where $Q_0^{(n)}$is taken as 1. Therefore, for a linear triangular component shown in Fig, the relationship between the shape structures and the related Lagrange polynomials 3.3a can be formed with the help of Eqs. 3.7 and 3.8 as

$$N_1 = Q_{p=1}^{(1)}L_1Q_{q=0}^{(1)}L_2Q_{r=0}^{(1)}L_3 = L_1$$
$$N_2 = Q_{p=0}^{(1)}L_1Q_{q=1}^{(1)}L_2Q_{r=0}^{(1)}L_3 = L_2 \qquad (3.8)$$
$$N_3 = Q_{p=0}^{(1)}L_1Q_{q=0}^{(1)}L_2Q_{r=1}^{(1)}L_3 = L_3$$

Similarly, for a triangular 2D quadratic element shown in Fig. 3.3b, the direction of the comp onent 2 and we can get the functions of form a Equation

$$N_1 = Q_{p=2}^{(2)}L_1Q_{q=0}^{(2)}L_2Q_{r=0}^{(2)}L_3 = L_1\ (2\ L_1\text{-}1)$$
$$N_2 = Q_{p=0}^{(2)}L_1Q_{q=2}^{(2)}L_2Q_{r=0}^{(2)}L_3 = L_2(2\ L_2\text{-}1)$$
$$N_3 = Q_{p=0}^{(2)}L_1Q_{q=0}^{(2)}L_2Q_{r=2}^{(2)}L_3 = L_3\ (2\ L_3\text{-}1)$$
$$N_4 = Q_{p=1}^{(2)}L_1Q_{q=1}^{(2)}L_2Q_{r=0}^{(2)}L_3 = 4L_1\ L_2 \qquad (3.9)$$
$$N_5 = Q_{p=0}^{(2)}L_1Q_{q=1}^{(2)}L_2Q_{r=1}^{(2)}L_3 = 4L_2\ L_3$$
$$N_6 = Q_{p=1}^{(2)}L_1Q_{q=0}^{(2)}L_2Q_{r=1}^{(2)}L_3 = 4L_1\ L_3$$

Similarly linear and quadratic tetrahedral elements (first order and second order) can be used to discretize a 3D domain.These element's numbering system is shown in Fig 3.3c, d.It is als o possible to write the shape functions for these elements using Eqs. 3.7 and 3.8 as

$$N_1 = Q_{p=1}^{(1)}L_1Q_{q=0}^{(1)}L_2Q_{r=0}^{(1)}L_3Q_{s=0}^{(1)}L_4 = L_1 \qquad (3.10)$$

and following the same steps for the other nodes,

$$N_2 = L_2,\ N_3 = L_3,\ N_4 = L_4 \qquad (3.11)$$

Similar to the quadratic tetrahedral component, it is possible to list the shape functions as

$$N_1 = L_1\,(2\ L_1\text{-}1),\ N_2 = L_2\,(2\ L_2\text{-}1),\ N_3 = L_3\,(2\ L_3\text{-}1),$$

$$N_4 = 4L_1\ L_2,\ N_5 = 4L_1\ L_3,\ N_6 = 4L_1\ L_4 \qquad (3.12)$$

Once the domain is discrete with great number of user's choice elements, any undetermined f unction ϕ within the component can be approximated with respect to the element coordinates and constant coefficients.

$$\phi_i^e = a_i + b_i x + c_i y \quad \text{for 2D} \qquad (3.13)$$

$$\phi_i^e = a_i + b_i x + c_i y d_i z] \quad \text{for 3D} \qquad (3.14)$$

Where i being the node number per element

$$i = 1, 2, 3, 4 \qquad (3.15)$$

Next, the unknown function can be interpolated for an element by solving the constant coefficients $(a_i^e, b^e_i, c^e_i$ and d^e_i in terms of π and also by solving the shape functions (N_i) for the specific element.

$$\phi^e = \sum_i^n N_i \Psi_i^e \qquad (3.16)$$

3.2.2 Computational Domain Discretization:

The ideal domain on which finite element method can be implemented must be discrete in a large number of small domains, called components. Such elements can be chosen in such a way that their shape and size closely suit the geometry and boundary curvatures of the related computational domain. All these small elements form a mesh which can be regular and irregular. The irregular mesh is very efficient in representing the desired domain compared to the regular mesh distribution. In regions of particular interest and other coarse materials, finer elements can be accommodated. It increases the precision of irregular meshing over normal meshing. In the thin, narrow and pointy regions where the electromagnetic fields differ rapidly, smaller mesh components should be considered for photonic computations. In areas where fields display an almost constant distribution, some computational elements may be sufficient. It is also very important to carefully select the shape and size of the boundary elements so that they can fit as far as possible the entire boundary structure. For this function, many basic geometries such as straight edge elements, iso-parametric elements, infinite elements and edge elements can be followed. The straight edge elements are triangles, rectangles and quadrilateral for 2D domains and tetrahedral, prisms, bricks and 3D domain pyramids. In territories with less rounded borders these are mostly useful. The iso-parametric or curvilinear elements have curvatures on the edges and their positional nodal coordinates are determined by the transformation of the local Cartesian coordinate into the global 6 finite element method for sensing curvilinear coordinates. These are useful for curved boundary geometries. For these types of component families, higher-order elements are also applicable. The infinite mesh elements can be very useful for an open-space or unlimited photonic problem. For the infinite components, the shape function decays exponentially in the directions where the field extends to infinity [27, 28]. In addition, the perfectly matched layer based on coordinate stretching can effectively truncate the computational domain resulting in the decline of the outgoing waves without reflecting to the computational domain.

3.3 Scalar Finite Element Method for Mode Analysis:

The major benefits of the scalar finite element method (SC-FEM) are the symmetric and small matrices generated in the calculations of the own value [29]. Furthermore, the spurious problem does not benefit from SC-FEM. SC-FEM, however, only delivers exact results when considering a homogeneous medium or, in other words, when assuming the boundary conditions, the field and its derivative are simultaneous. Here we explore using the SC-FEM

to evaluate a 2D cross-sectional waveguide. However, the complete vector analysis is worked out later in this chapter throughout the evaluation of the penalty function technique and the vector finite element method is introduced. Vectors are the field functions that are contained in the edges of the object. In SC-FEM, where the field values are stored in nodes, the nodal finite element is used.

There are two ways to solve optical waveguide problems: the methods of variance and the residual methods measured. Both methods yield equations of their own value that need to be resolved. [20, 30–32]

The mathematical domain shown in Fig 3.4 in the methods of variation. The number of sections is divided and the law of variance is modified to the sum of the discrete functions of all segments. The solution of the waveguide problem requires already understanding the function in the variation theory. The governing partial differential equation of the propagation of electromagnetic waves is already established, contrary to the variational theory. Therefore, in solving the electromagnetic wave equations, the weighted partial methods, particularly the Galerkin method, are very important.

3.3.1 Galerkin Method:

The Galerkin method is one of the most popular and powerful numerical techniques for solving transient partial differential equations of parabolic type. The Galerkin method can be viewed as a separation-of-variables technique combined with a weak finite element formulation to discretize the problem in space. This leads to a stiff system of ordinary differential equations that can be integrated by available off-the-shelf implicit ordinary differential equations (ode) solvers based on implicit time-stepping schemes such as backward differentiation formulas (BDF) or implicit Runge-Kutta (IRK) methods.[33,34]

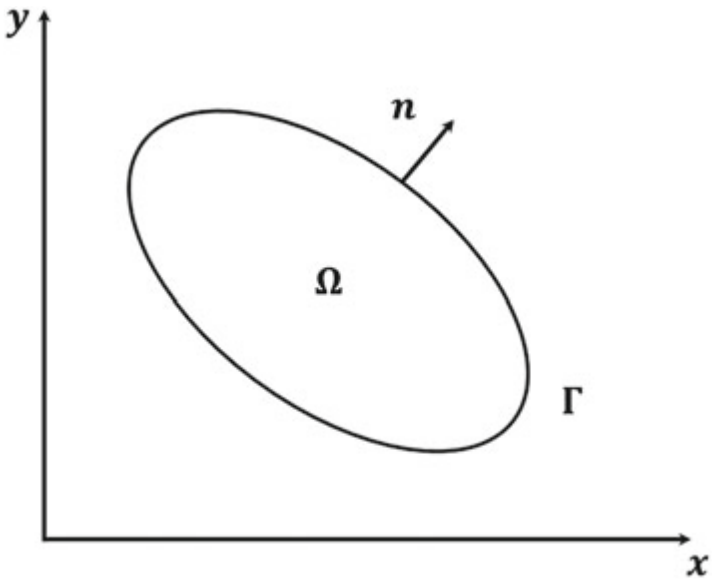

Fig 3.4: Analysis domain [28]

The Galerkin method is used in this section to obtain the efficient index neff by solving the formula of the scalar wave.

$$\frac{\partial}{\partial x}\left(p\frac{\partial \phi}{\partial a}\right)+\frac{\partial}{\partial y}\left(P\frac{\partial \phi}{\partial y}\right)+k_0^2(q-n_{eff}^2\mathrm{p})\phi=0 \qquad (3.17)$$

	φ	p	q
TE-wave	E_x	1	ϵ_r
TM-wave	H_x	$1\ \epsilon_r$	1

Where ϕ is the wave function, k_0 is the free-space wave number, and ε_r is the material permittivity. E_x and H_x are, respectively, the electric field and magnetic field in the *x*-direction.

3.3.2 Weak Galerkin Formulation

A spatial weak formulation of the model problem is obtained by multiplying the parabolic equation (1) by a test function v in the Sobole v spaceH_0^1, integrating over (0,1) and integrating by parts to show that u∈H_0^1 satisfies

$$\begin{cases}(v,u_t(.,t))+A(v,u(.,t))=(v,f(.,t)),\forall\, v\in H_0^1, 0\le t\le T,\\ u(x,0)=g(x), x\in(0,1),\end{cases} \qquad (3.18)$$

Where,

(v, u(.,t))= $\int_0^1 v(x)u(x,t)dx, A(v,u(.,t))=\int_0^1[a(x)\frac{dv(x)}{dx}u_x(x,t)+b(x)v(x)u(x,t)]dx.$

3.3.3 Assessment:

For test the finite element analysis, a simple example is to calculate the cutoff number of an air-filled rectangular waveguide shown in Fig. 3.5.

This problem is a perfect evaluation of the proposed method. It has an exact solution in which the SC-FEM output can be tested. Even, since the waveguide medium is a homogeneous product and the surface is surrounded by a great electrical conductor (PEC). For this type of problem, SC-FEM is the excellent choice. The waveguide width is set to a= 1.2 μm and the height is set to b=1 μm. The wavelength of the simulation is 1.5 μm. We can calculate the exact solution of the cutoff number effectively from the following relationship:

$$kc_{mn} = \sqrt{\left(\frac{m\pi}{a}\right)^2 + \left(\frac{n\pi}{b}\right)^2} \qquad (3.19)$$

Where m and n are Eigen numbers that take integer values 0, 1, 2. Depending on the width and height of the wave guide presented the fundamental cutoff for TM-wave (m = 1, n = 1) equals Kc_{11} = 4.089437167421735 (rad/m).

The mathematical domain is divided into triangular elements of first order for the first-order component. Then, the global matrices are configured after evaluating the local matrices. Since the wave function ϕ is zero at the wave guide boundary, it is advantageous to decrease the order of the assembled matrices by replacing the rows and columns corresponding to the nodes at the boundary. Lastly, the equation of its own value Eq. 3.17 a β value of its own is solved. It is therefore possible to evaluate the cutoff number numerically using the following relationship:

$$kc_{mn} = \sqrt{k_0^2 - \beta_m^2 n} \qquad (3.20)$$

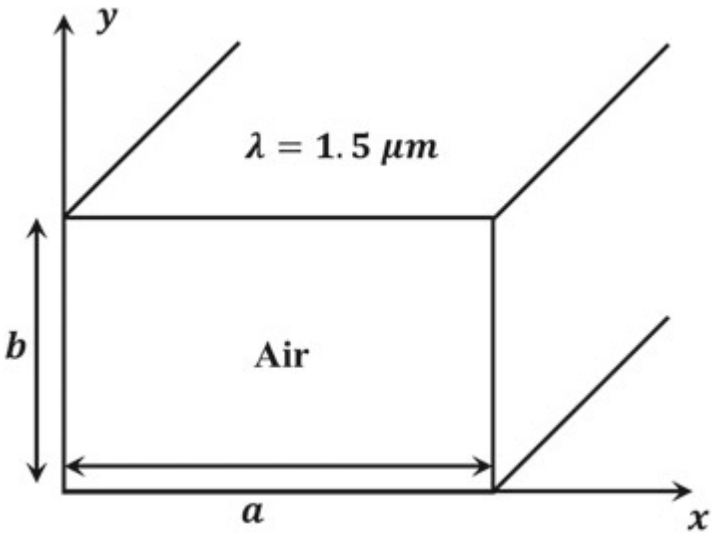

Fig. 3.5 Air-filled rectangular metallic waveguide. [35]

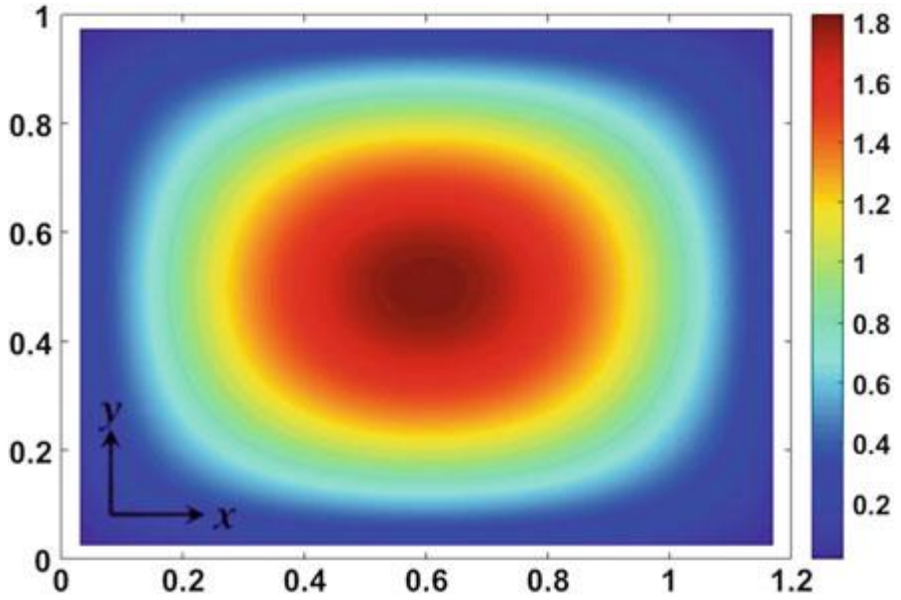

Fig. 3.6 Fundamental mode. [35]

The computational domain is discretized into 800s order elements that produce 1521 unknowns for the second order triangular element. The cutoff number determined under these assumptions is Kc_{11} = 4.089451948101586 rad/m with an error of e=0.000014780679851. As can be observed, the error produced by the element of the second order is much lower than that generated using the element of the first order, while using less unknowns.

3.3.4 Perfectly Matched Layer:

The development of a functional FEM solver includes the simulation boundary effects to be included. As discussed above, simple FEM boundary conditions set the field and its normal derivative at the simulation area boundary to zero that can be assumed as the computational domain is in a metal box or magnetic box [31]. This approximation is generally not true as sometimes in open boundaries we need to simulate the structures. A perfectly matched layer (PML) artificial absorbing boundary condition is used [36]. For wave equations, it is a non-physical surface. It is usually used to truncate region of study to mimic conditions of open boundaries. It is made to match the nearby domain as it can be noticed from its name "perfectly matched." In other words, it is not permitted to represent the incident waves on the PML. This function helps the PML over any other material that is absorbent. This property allows the PML to absorb outgoing waves from the computational domain's interior effectively. It works without reflecting them back into its domain.

In 1994, the Berenger team created the first PML for use with Maxwell's equations called "split-field PML [36]." Many adapted versions of PML have been developed for Maxwell's equations and other wave equations including Schrodinger's equation since then. The PML divides the electromagnetic field into two components of the non-physical field in the PML region. Later, due to its efficiency and simplicity, a further improved formulation called uniaxial PML or UPML has gained popularity [37]. UPML is described as a material that absorbs artificial anisotropies. While both UPML and split-field PML were briefly derived from the development of conditions that force no reflection from the incident plane waves. Both formulations later proved to be comparable to a neater approach called stretched coordinate PML [38, 39]. This approach uses the so-called transformation of the coordinate. The transformation of the coordinate maps one (or more) coordinate to a complex number. In essence, this method is like an empirical continuation of the wave equation into complex coordinates, replacing the propagating wave with an exponential decay.

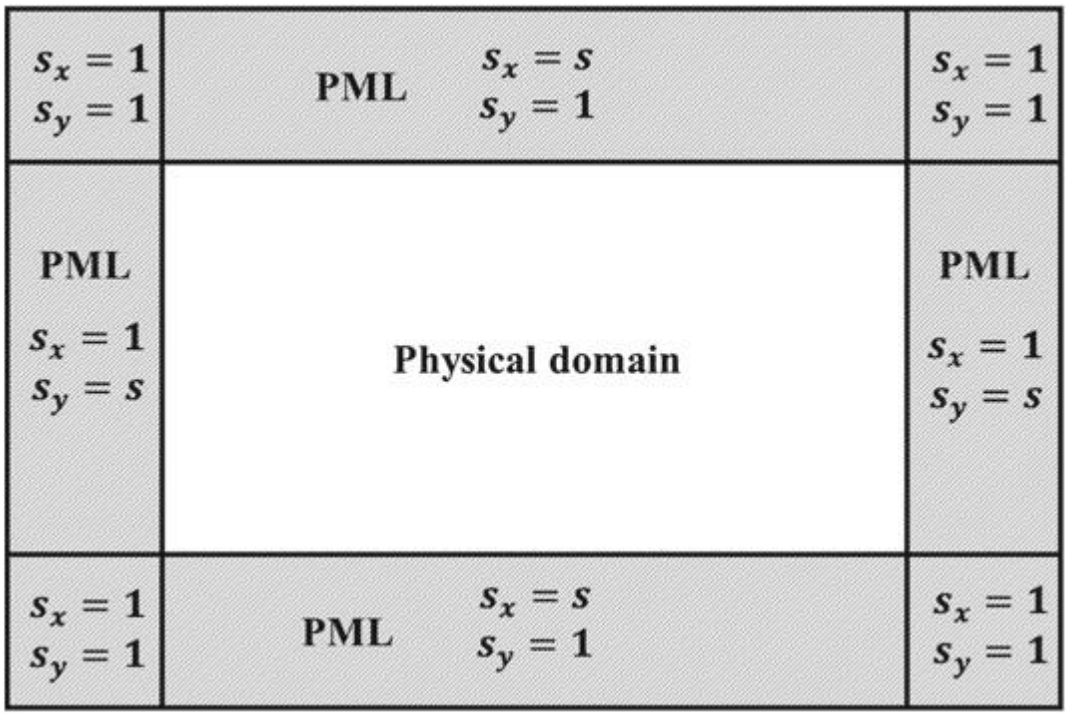

Fig 3.7: Definition of the PML parameters $s_x$and s_y [49]

3.3.5 Variations of the Conventional FEM:

Many FEM analyzes rely on the triangular component of the second order because of the poor accuracy of the triangular element of the first order [40–43]. However, the additional nodes between the pairs of triangular vertices cannot be adjusted to the boundary of a curved structure for the conventional second-order element. Using curvilinear elements, this problem has been solved. Curvilinear component approach converges more easily to curved structures compared to conventional ones [44]. Moreover, due to its computational simplicity and ease of adaptive mesh refinement, the first-order component is often preferred. In addition, most mesh generation code relies on triangular elements of the first order.

As a result, several research efforts were devoted to enhancing the accuracy of the element of first order. Recently a new new technique has been developed. It is called "smoothed Galerkin" [45, 46]. This new technique is based as in mesh-free methods on weakening the weak form (W2) [28]. In addition to approximating the field factor, W2 also shapes field derivatives through the gradient smoothing technique [48]. The most important features of the W2 form are the high precision and the less sensitivity to mesh distortion. Using the smoothed Galerkin form, which introduces a novel class of so-called smoothed finite element method (SFEM). It is for various mechanical problems, will improve the accuracy of any system based on the Galerkin model. In the traditional FEM, the shape function derivatives at component

boundaries are numerically discontinuous, resulting in poor output of FEM. In SFEM, this drawback in FEM was smartly overcome by approximating the derivatives to continuous component boundaries. The SFEM was recently introduced for photonic interface time domain analysis [49, 50].

3.3.6 Time Domain Methods:

The steady progress in the field of Nano-photonics has triggered in numerical methods. A sequence of fundamental research that could cope with this steady progress. Similar numerical methods are used in both ways to solve Maxwell's equations: frequency and time domains. Maxwell's time domain approach receives a great advantage over the frequency domain solution. This advantage is represented in the ability in a single simulation run to cover a wide range of frequencies. Time domain methods also give the actual behavior of the light-photonic structure interaction.

Therefore, in real-time situations, these methods are important for design and performance prediction. A very powerful and flexible approach is the Finite Difference Method (FDM)[25].From its mathematical simplicity and its applicability to several photonic problems, it gained its reputation. A time domain method called "finite time domain difference (FDTD)" was introduced on the basis of the FDM [25]. The FDTD was commonly used in photonic device modeling. It has also been extended to include various types of materials such as anisotropic, dispersive, and nonlinear materials. It suffers from inefficient discretization of irregular geometries. This disadvantage is opposed to precise modeling of complex photonic structures and curved geometries such as photonic fiber structures. This problem is commonly referred to as "the problem of stair casing." Besides this problem, the modern FDTD has issues with stability. The size of the time stage should follow the Courant – Friedrichs – Lewy condition, which renders the FDTD highly sensitive to the option of phase length. These condition decreases the time stage size used and therefore increases the total processing time. Various modifications of the FDTD have been suggested to overcome the problem of stability. A FDTD-BPM has been implemented based on the time domain beam propagation method (TD-BPM). TD-BPM eliminates the rapidly varying field element, leaving to simulate only the slowly varying field [51, 52]. Such approximation has made it possible to use a moderate time step size. A complex framework alternating indirect path technique (CE-ADI-FDTD) and split step technique (SS-FDTD) were also proposed to use large time stage length [26,53]. CE-ADI-

FDTD and SS-FDTD, unlike the FDTD-BPM, rely on simulating the coupled Maxwell equations that contain three coupled equations to be solved at each time step, resulting in higher computational costs.

3.4 Finite Element Time Domain:

Instead, the approach of finite elements (FEM) gives a genuine solution to the problem of stair casing. It is capable of discretizing the computational domain into triangular elements and modeling curved and complicated geometries accurately. Over the past decade, a number of time domain finite element (FETD) methods have been implemented. Generally speaking, the nodal FEM and the edge FEM are two types of FEM methods. The unknown field is stored at the vertices of the element in the nodal FEM. The unknown field is stored at the edges of the element instead of its vertices in the edge FEM. The later has the ability to include the boundary conditions correctly, but it also benefits from the resulting matrices of its unconditioned form. On the other hand, well-conditioned matrices and also a better convergence value are provided by the nodal FEM. Based on the edge-based functions, Maxwell's time domain equation is a vector solution. However, it generates a conditionally stable behavior identical to FDTD. On the other hand, a solution has been presented to the curl-curl wave equation. It solves one of the field vectors of Maxwell's equations [55]. This method is unconditionally stable. It contains a large system of equations that must be resolved at every step of the time. It is considered expensive in terms of computation. It also generates matrices that are well-scaled. The functions of nodal form are known to be computationally efficient. A solution to Maxwell's time domain equations is made based on the nodal shape function by applying TD-BPM which allows the use of moderate time phase length. FETD approaches can be classified into explicit and implicit schemes based on nodal shape structure. A mass lumping technique is used in the explicit scheme and the slowly varying wave equation is temporarily dis-created using the formula of the central finite difference [32]. No linear equation system is solved in this scheme at each time step. One of the major drawbacks of this method is that it provides a conditionally stable time-marking algorithm. The time-step size should satisfy the condition of Courant–Friedrichs – Lewy to ensure the algorithm's stability. In fact, the method's reliability is severely affected by the mass lumping technique used. The second scheme dis-creates the slowly varying equation of the wave in the time domain, giving rise to a linear system of equations to be solved at each stage. The benefit of the second scheme is that the time-marketing algorithm

generated is unconditionally stable, allowing for the use of moderate time steps. Using either the unconditional stable Newmark-beta scheme or the Padé approximation [40, 49], this scheme can be implemented by discretizing the slowly varying wave equation. The latter algorithm needs less memory because, unlike the Newmark-beta method. It uses only the previous one to calculate the field in the next time stage.

3.4.1 Single Mode Slab Waveguide (Perfectly Matched Layer Assessment)

The first measurement considered is the single-mode slab waveguide shown in Fig. 3.8. The waveguide is excited by a pulse with a z-directional Gaussian profile and a transverse φ_o profile corresponding to the planar waveguide's basic mode. Therefore, the initial field at $t = 0$ is taken as:

$$\varphi_0(y, z, f = 0) = \phi \circ (y)\exp\left[-\left(\frac{z-z_0}{w_0}\right)^2\right]\exp[-j\beta(z - z_0)y] \quad (3.21)$$

Where z_o is the initial pulse position, and W_o is the spot size and β is the propagation constant of the fundamental mode.

Figure 3.8 indicates the TE area during the simulation on the control line at a different time. Figure 3.8 displays the calculated power during the simulation at each time level. Such a figure shows the method's stability. In figure, the energy during the simulation is constant and uniform to 1 which means that the system does not have a non-physical amplification. Until the propagated pulse reaches the PML as shown in Figure 3.8. The energy starts dropping down as an indicator that the incident pulse is efficiently. It has absorbed with limited reflection within the PML.

3.4.2 Applications

In computational modeling of photonic devices such as biomedical sensors, the use of complete vector approaches is essential and polarization handling devices including plasmonic structures, polarization rotators, polarizers, polarization filters, polarization splitters, and couplers [54-65]. In this examination, the FV-FEM is utilized to demonstrate and dissect surface Plasmon photonic precious stone fiber (PCF) biosensor. Figure 3.9 shows the cross area of the recommended PCF biosensor. The proposed model of PCF is based on the use of two rings of air holes with a central air hole in the core area. The outer ring air holes have a small diameter d_1 and are arranged with a hole pitch in hexagonal shape. A range d_2 moves the

two air holes along the x-axis, as shown in Fig. 3.9. The inner ring air holes have elliptical shape with smaller and larger diameters of 2a and 2b, respectively, the central hole has a d_c diameter. The air holes in the inner ring are used to monitor the containment through the central area of the two core-guided modes. Johnson and Christy obtained the gold permittivity [66].the suggested design has a silica background material which has the following Eq:

$$n_s^2(\lambda) = 1 + \frac{B_1\lambda^2}{\lambda^2 - C_1} + \frac{B_2\lambda^2}{\lambda^2 - C_2} + \frac{B_3\lambda^2}{\lambda^2 - C_3} \qquad (3.22)$$

Where n_s is the silica refractive index and where λ is the μm wavelength. Additionally, B_1, B_2, and B_3 are given by 0.6961663, 0.4079426, and 0.8974794, while C_1, $C2$, and C_3 are equal to 0.00467914826 μm^2, 0.0135120631 μm^2, and 97.9340025 μm^2, respectively. In this test, the VFEM is used to find the suggested biosensor's quasi-TE and quasi-TM core-guided modes and plasmonic modes. [54]

3.4.3 Common FEM Applications

*****Mechanical/Aerospace/Civil/Automotive Engineering

*Structural/Stress Analysis

- Static/Dynamic
- Linear/Nonlinear

*Fluid Flow

*Heat Transfer

*Electromagnetic Fields

*Soil Mechanics

*Acoustics

*Biomechanics

3.5 Device Geometry:

Our proposed device's schematic structure is shown in Figure 1. The main device of our interest is two silicon cores. It is separated by a narrow slot region displayed by a dashed red box. The lightweight straight resonating design, vertically slotted, is equipped with two combined bus waveguides in and out. Through one bus waveguide, light from a switchable laser source travels and excites the slotted structure at a specific wavelength. The three output facets of the in / out bus waveguides which will select the corresponding resonating wavelength (λres). Electromagnetic energy builds up in the slot cavity during the resonance and the resonance wavelength. It can be detected from both facets of the output bus waveguide ($\lambda out1$ and $\lambda out2$) as well as from the opposite end of the input bus waveguide. The photodetectors detect the response from the output integrated waveguide. The silicon slot guide is isolated from the silicon substratum by a silicon dioxide (SiO2) buffer layer.

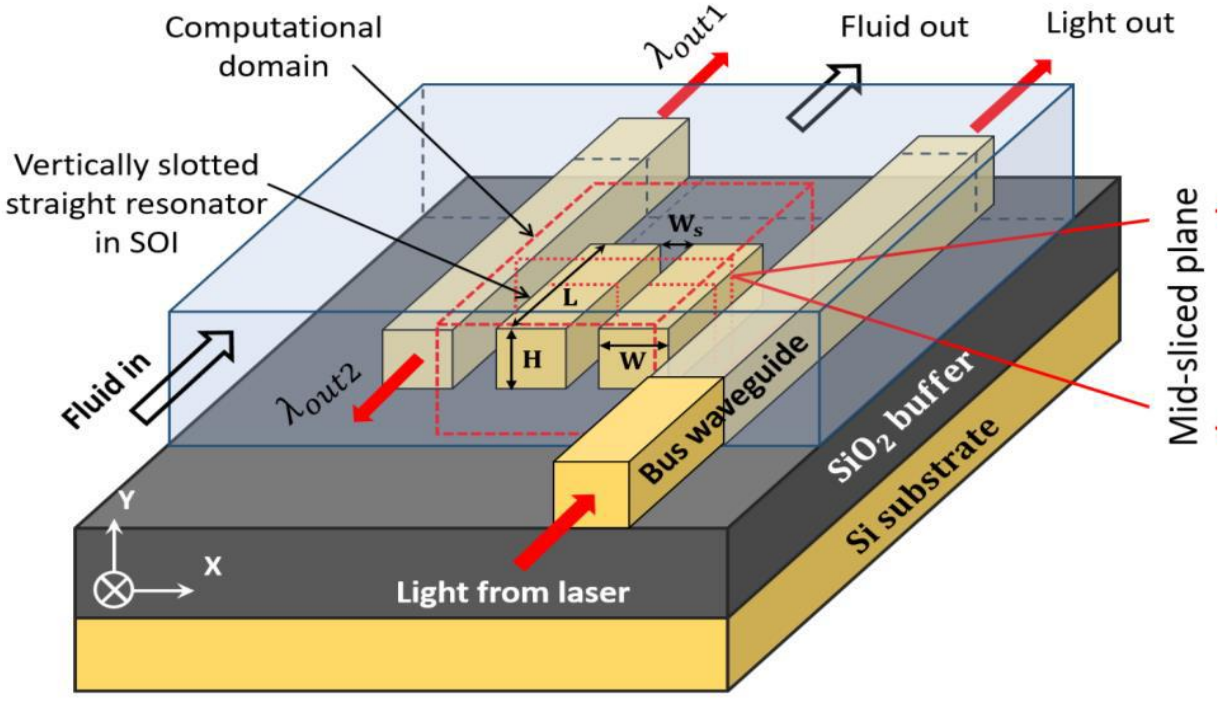

Fig 3.8: Three dimensional schematic diagram of single vertically-slotted straight resonator. Red dashed box is showing the computational domain. Insets are showing the mid-sliced plane with dominant Ex field profile along x-axis shown by black lines. [70]

The silicon and silicon dioxide refractive indices are taken as n_{Si} = 3.476 and n_{SiO2} =1.44, respectively at the 1550 nm operating wavelength. The proposed device's primary visible advantages can be explained in three measures.

First, due to Nano-scale dimensions, the compact design of the device results in high-scale integration and manufacturing facility compared to other complex devices. Second, there is a significant advantage over traditional rib and Nano-wire structures in the slotted resonating structure. The quasi-transverse-electric (TE) mode's dominant E_x field increases within the slot region. It allows for a strong light-analytic interaction instead of just using the evanescent field tail for sensing. Third, with the help of the first two points, a much-improved performance such as sensitivity (S) and detection limit (DL) can be achieved. The slot and the surrounding region can be filled with low-refractive, non-linear and organic materials. Here the efficiency of the proposed device is presented by using the low-indexed saccharose solution in the slot and cover medium as a chemical sensor representing the 3D slotted resonating structure. We also characterized the device as a bio-sensor immersed in water where a 5 nm ultra-thin (T_s) bio-layer with refractive index 1.45 has been considered. Compared with other alternative photonic sensing systems, the manufacturing process of our proposed system compatible with CMOS without a curved section can be easy. By etching two straight Si rails into a commercially available SOI wafer, the vertically slotted structure of silicon can be easily manufactured. Therefore, the plasma-enhanced chemical vapor deposition (PECVD) will achieve further growth of the top Si layer on the SiO2 buffer layer. The Si layer's height can be modified by precisely monitoring or increasing the rising time. A thin photographic film for patterning is deposited on the Si substrate. Reactive ion-etching (RIE) is then used to render the two Si strips interspersed with a slot area. Due to the presence of sensing material with different refractive index values, the rigorous investigation of design parameters, calculation of dominant and non-dominant field components. The profiles for the basic quasi-TE and TM modes are of great importance when we design a sensing device. Our two-dimensional (2D) in-house and newly developed three-dimensional (3D) finite element method (FEM) are used as mathematical methods to obtain the Si slotted resonator's modal solutions. A short length of straight vertical slot waveguide is the 3D slotted resonator. As a result, the use of the computationally efficient fully vectoral rigorous 2D-FEM can estimate a part of the design parameters. [70]

Chapter 4

Comsole Mutiphysics

4.1 Introduction:

Comsole Multiphysics is a cross-platform finite part analysis, solver and Multiphysics simulation software package. It permits typical physics-based user interfaces and connect systems of partial differential equations. Comsole software gives us Integrated Development Environment (IDE) and undivided system for electrical, mechanical, fluidic, acoustics and chemical applications. [1]

Here, we used this software for silicon slot wave guide based sensors simulation. Our all simulations are 2D simulation. This software can simulate 1D, 2D, and 3D simulation.

4.2 Comsole User Guide Line:

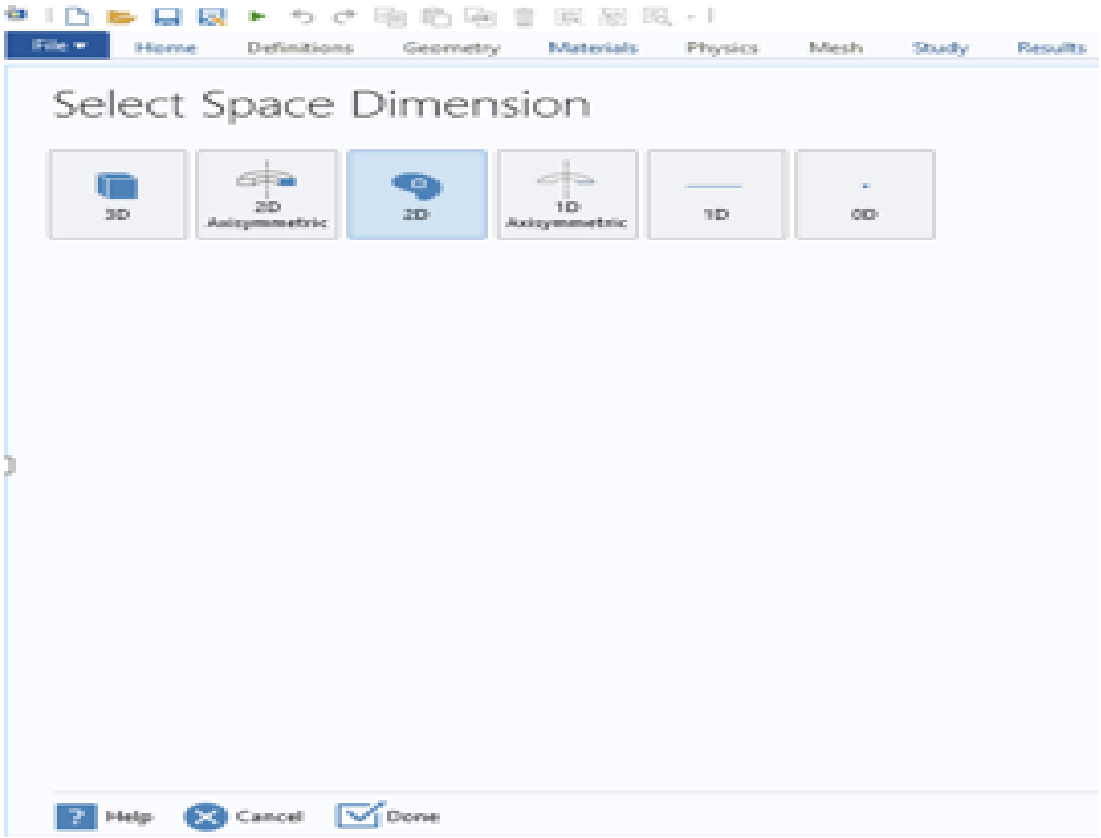

Fig 4.1: Space Dimension

At first we need to open new file in Comsole then we go Model Wizard and Select Space Dimension in 2D.

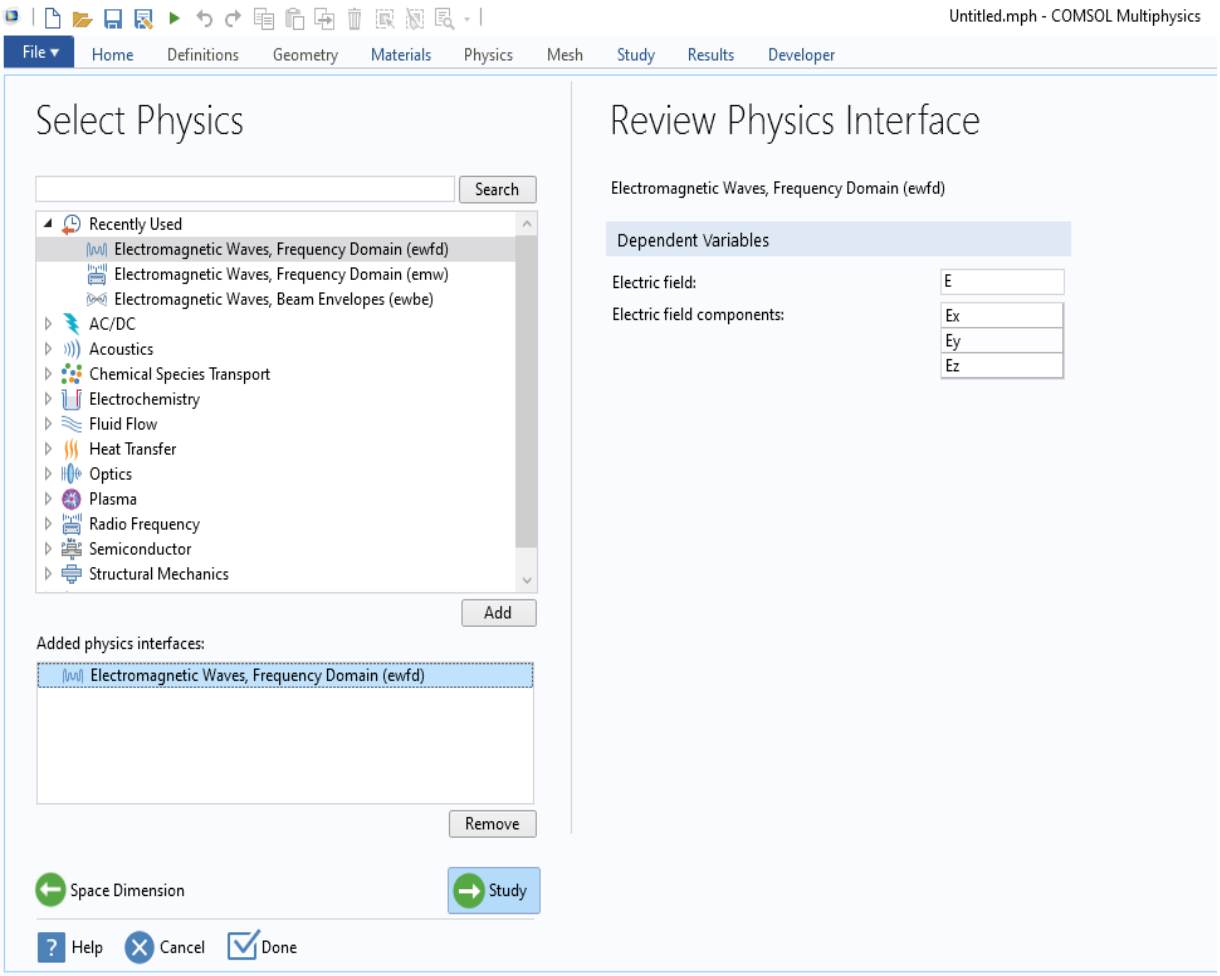

Fig 4.2: Select Physics.

Then, we go to optics then Wave optics and add Electromagnetic Waves, Frequency Domain (ewfd). Then we click study for save this part.

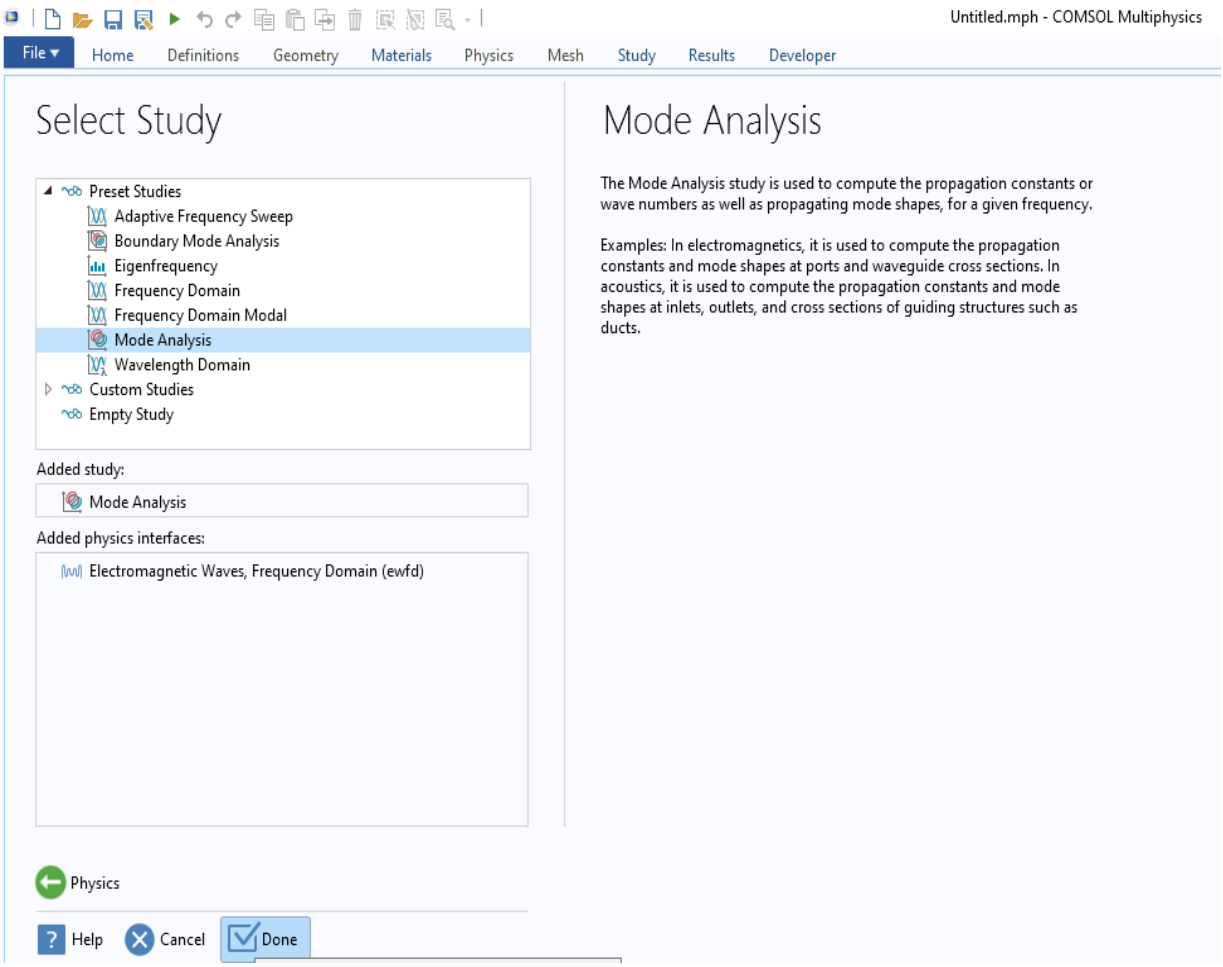

Fig 4.3: Mode Analysis

Then, we need to go Model Analysis next go to Global Defination and also select the perameters step by step.

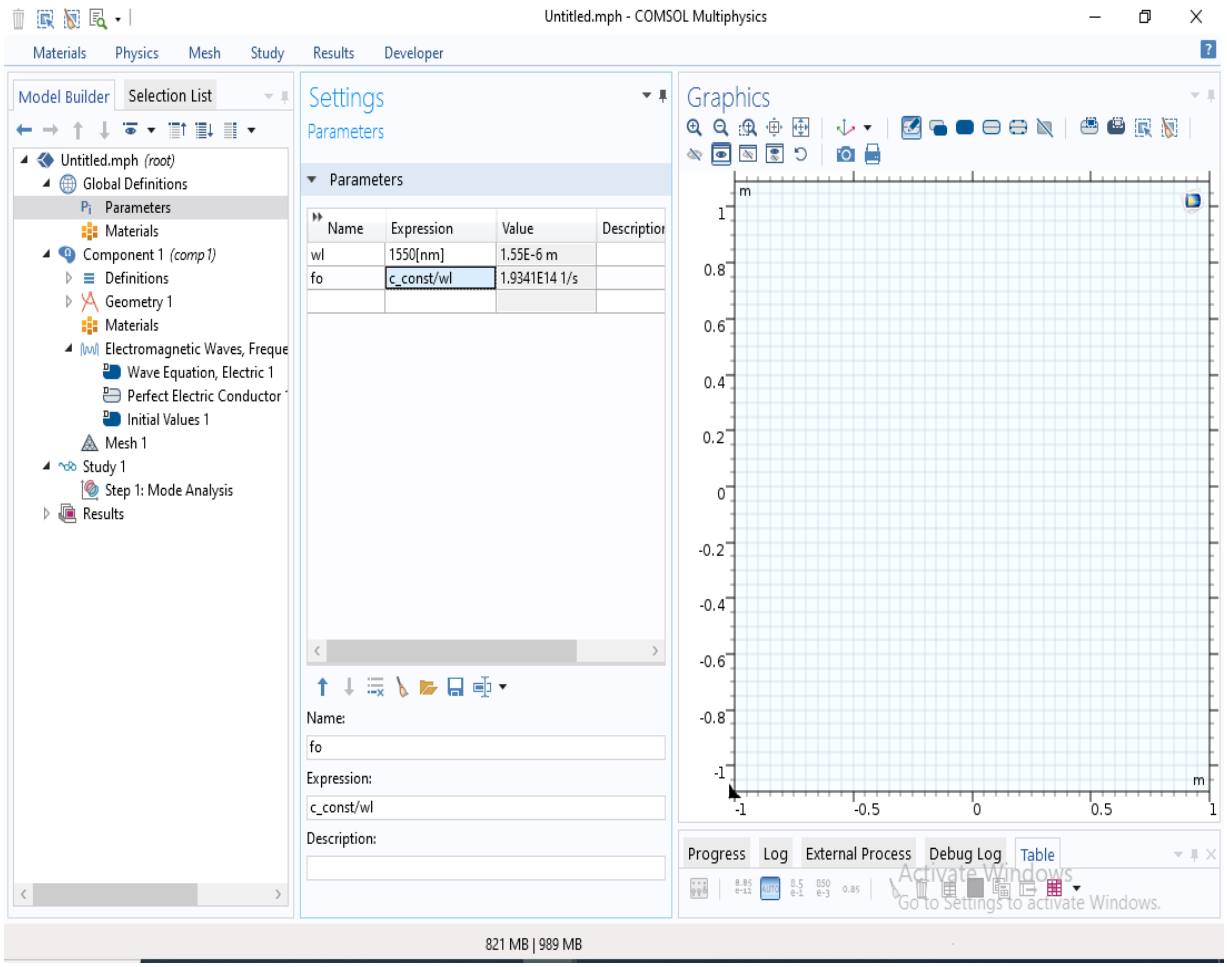

Fig 4.4: Parameters Selection

Table 4.1: Parameters for Air slot waveguide

Wavelength(wl)	1550 nm
Height (H)	150 µm
Core width(W)	100 µm
Slot width(Ws)	100 µm
Frequency(fo)	C_const/wl

Here we used all of these parameters for Air slot waveguide.

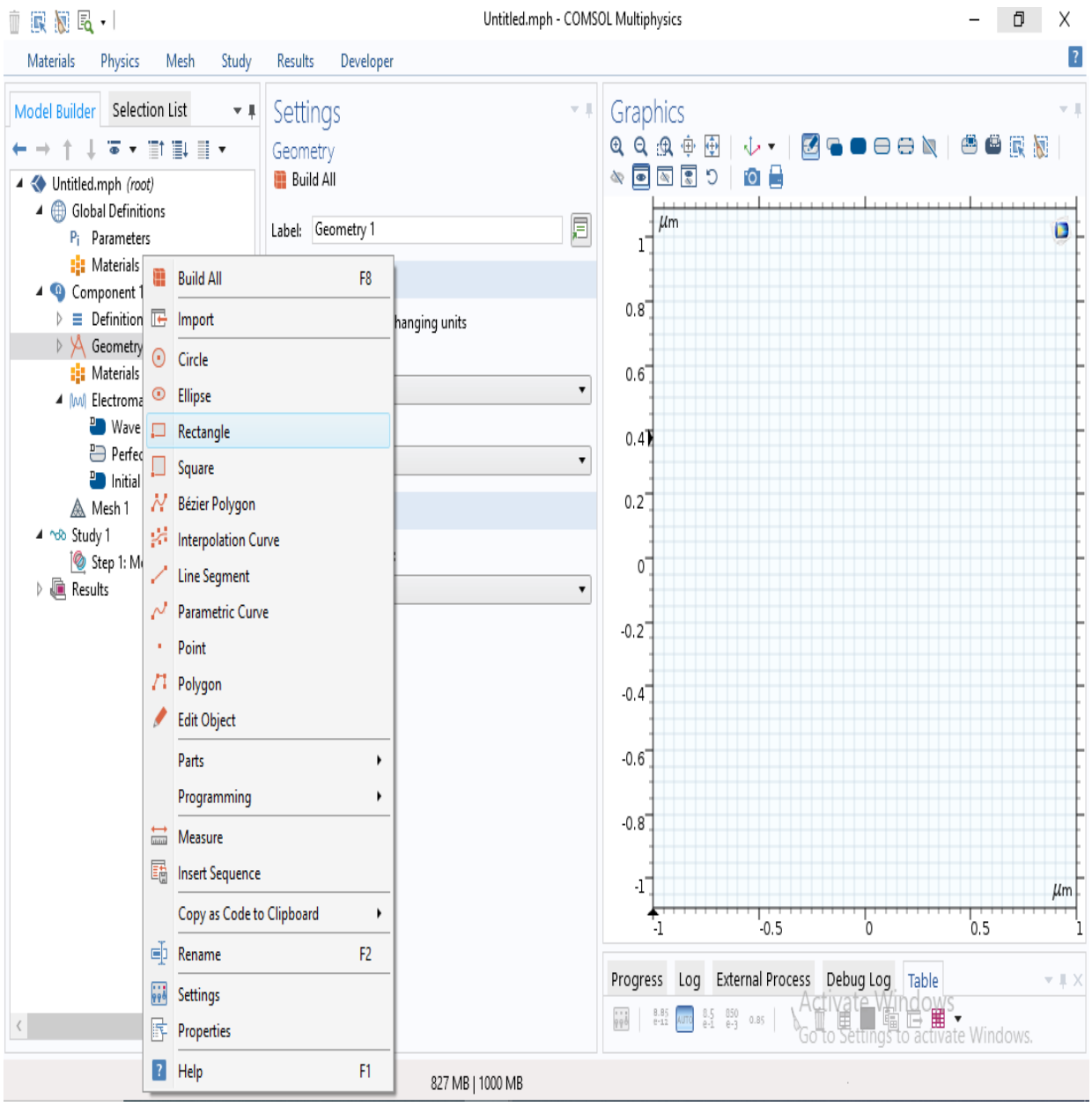

Fig 4.5: Geometry Selection

Now we need to select Geometry the Component. Here we used rectangle for our simulation.

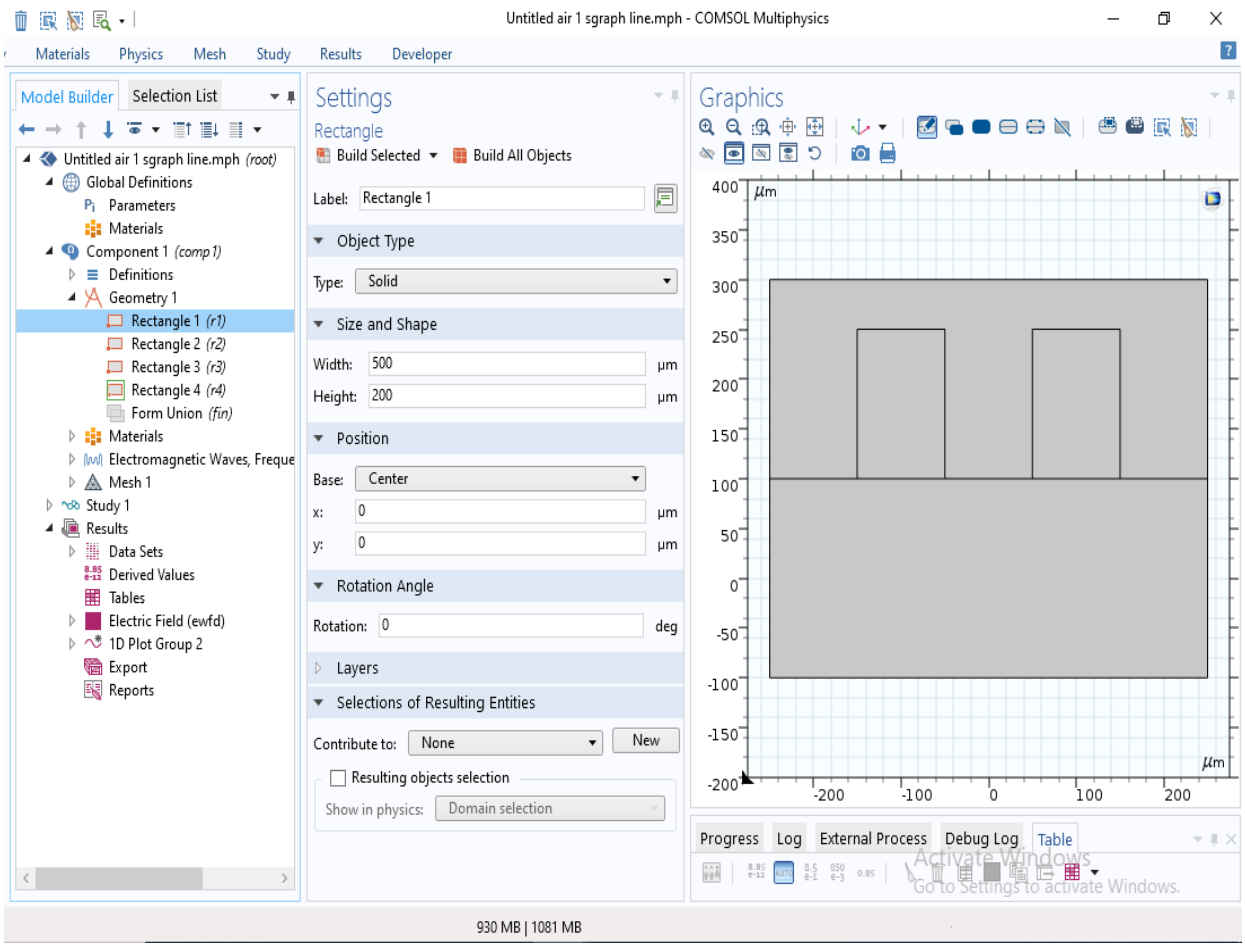

Fig 4.6: Geometry Type Selection

Now we need to create Geomeatry for our simulation. Here we provided geomerty height, width, type and position. We create one by one desire numbers of geometry for the simulation.

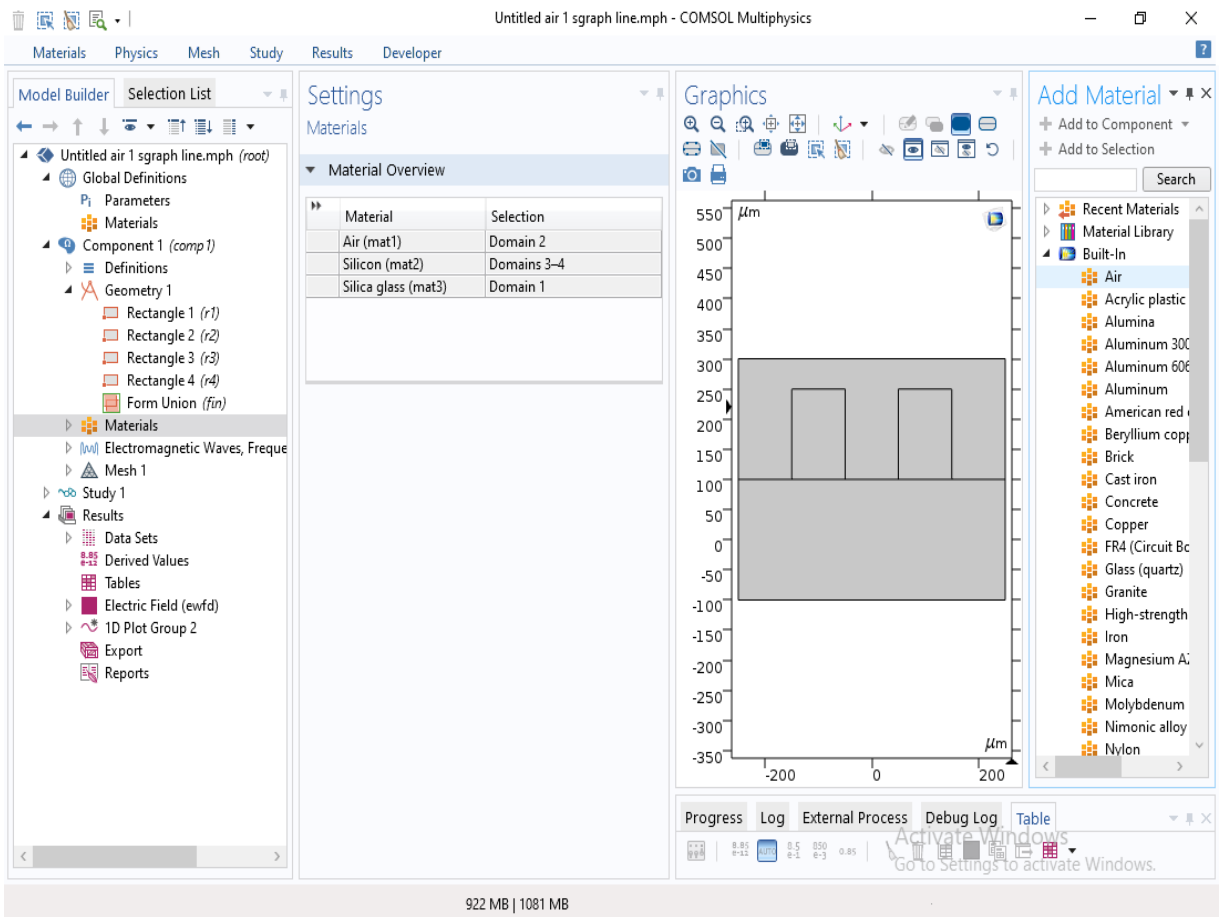

Fig 4.7: Addying Materials

Next step we added materials Air, Silicon and Silica Glass for our simulation.

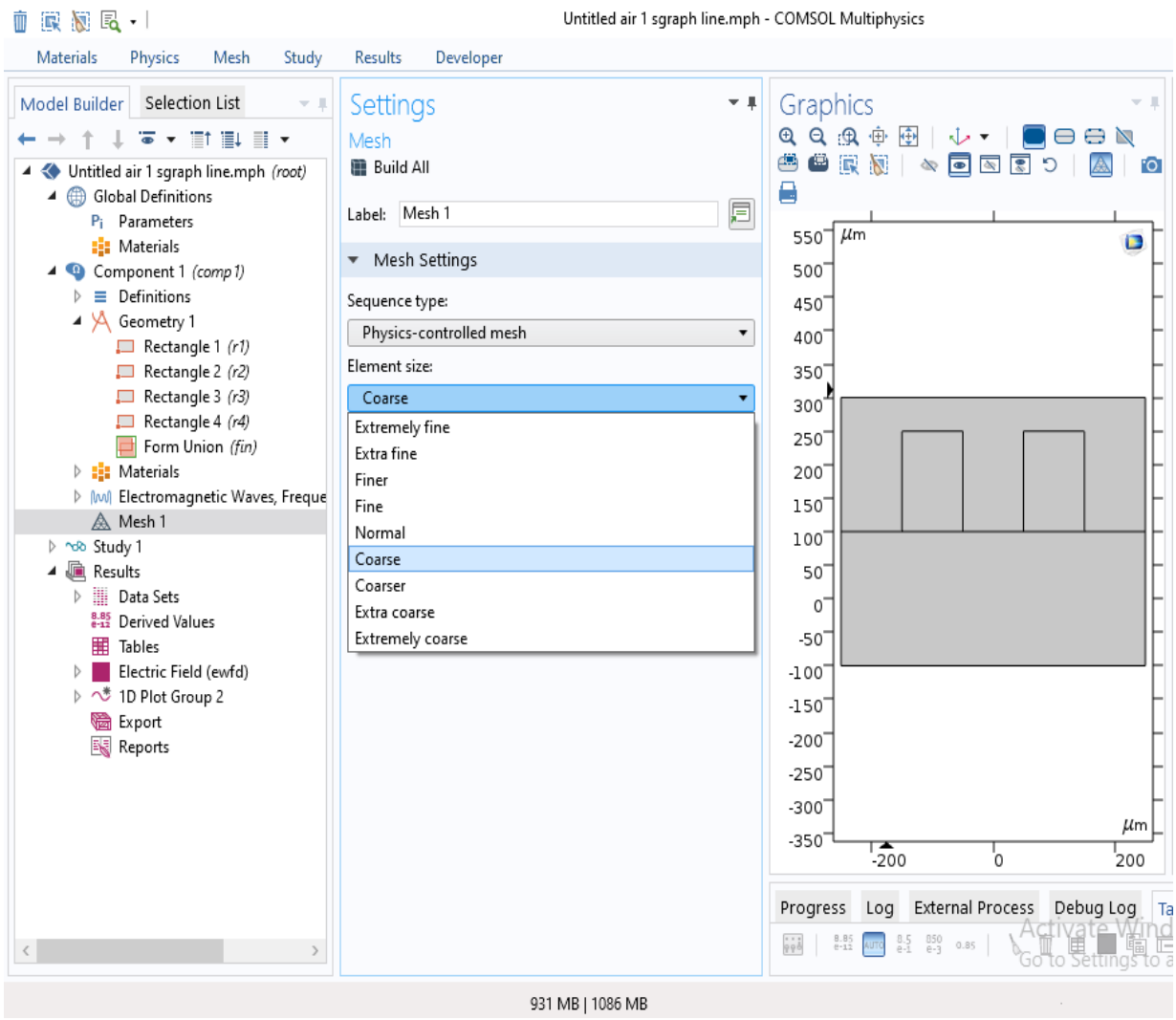

Fig 4.8: Mesh Setting

Then we first take Physics control mesh and added Element size. We taken element size in Coarse.

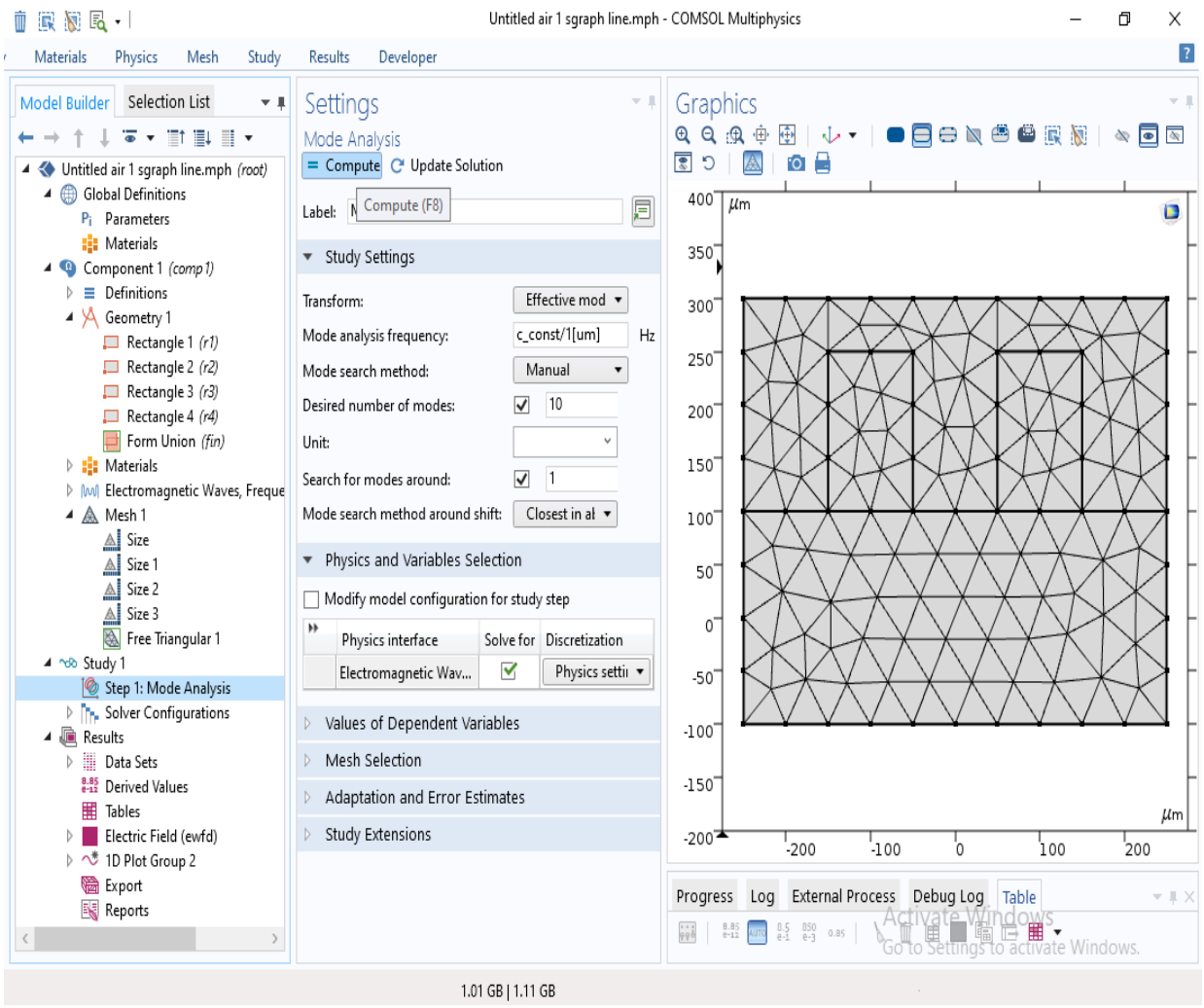

Fig 4.9: Adding Modes

Here we take desire number of modes 10. But desire number of modes can be any number. Then we need to Compute Solution.

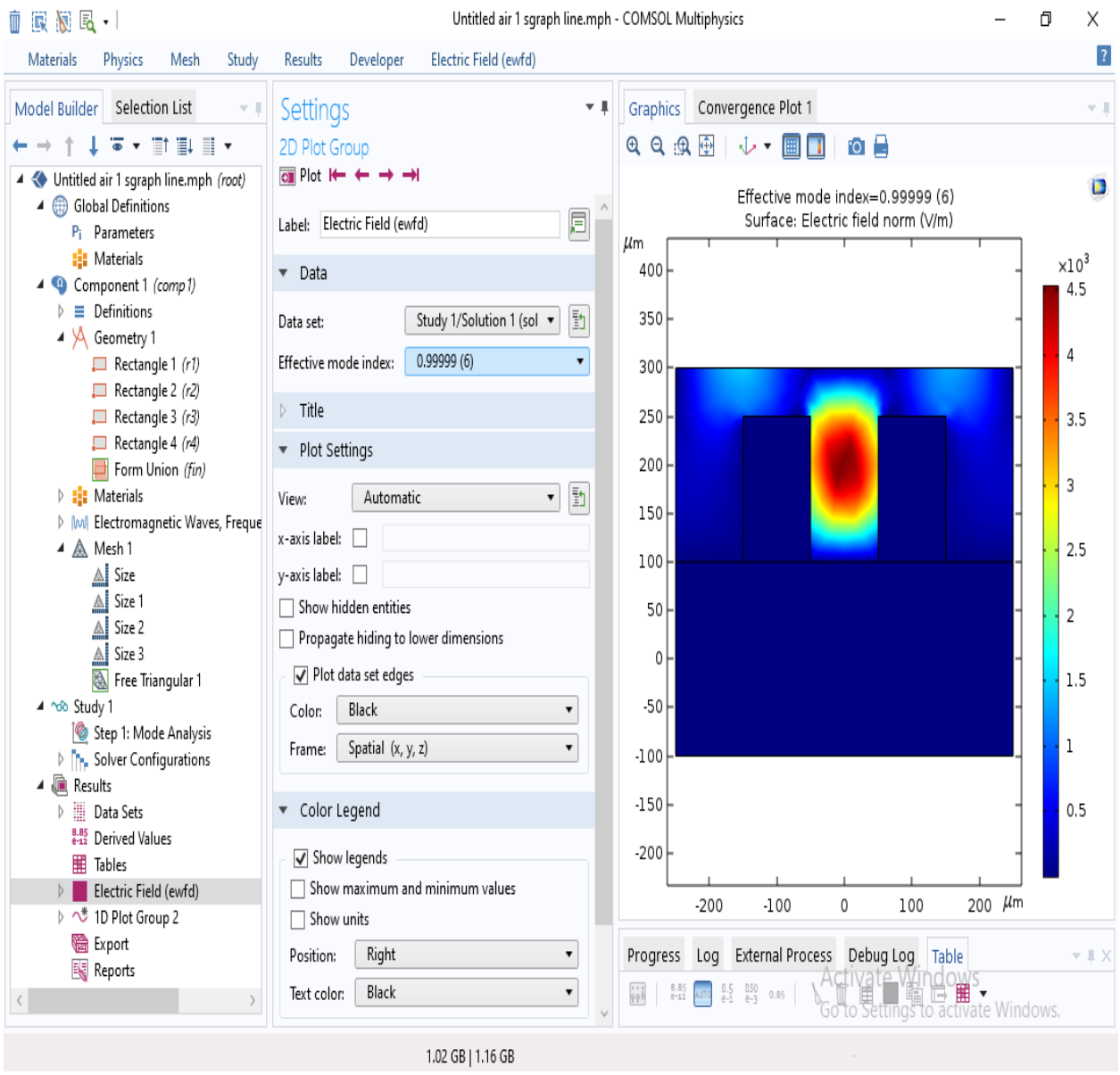

Fig 4.10: Results in Electric Field

Finally we go to the results and check Electric Field. Our simulation result given in Fig 4.10. This is the result for Air simulation by using Silicon Slot Waveguide.

Chapter 5

Simulation and Results

This Simulation is done by COMSOL Multiphysics Software. COMSOL Multiphysics is a finite element analysis based solver and Simulation software package for varieties of engineering and physics based applications, particularly for coupled phenomena. COMSOL Multiphysics additionally allows for entering coupled process of partial differential condition, other than ordinary material science based User interface. COMSOL Multiphysics software works with optical fiber modal analysis in waveguides using finite element process for solving refractive index mode. The biggest challenge in this chapter to simulation of water, salinity variation with refractive index and air, methane, CO_2 refractive index variation.

Simulation of a slot waveguide as a Salinity sensor**:**

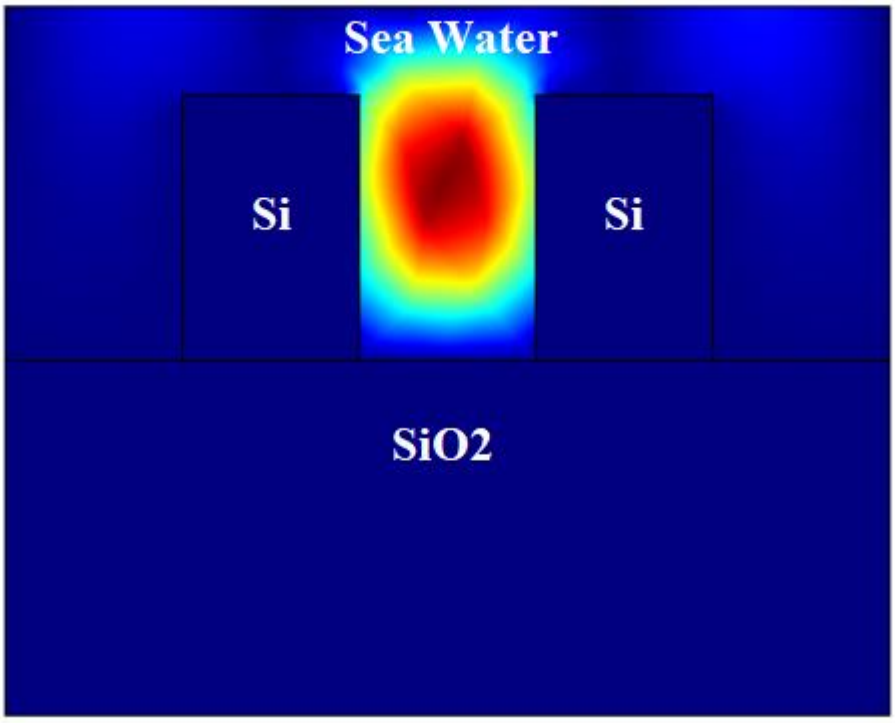

Fig 5.1: Simulation of Salinity in a slot waveguide

The experimental demonstration of a slot-waveguide based chemical and biochemical sensors. Refractive index sensors based on planar waveguides play a prominent role in chemical and biochemical analysis. This label-free sensing process can be provide real-time results with the minimum sample preparation. A change in refractive index of the penetrate region reason a corresponding phase shift can be detect as a frequency or intensity shift which is convert to the sensing signal. The use of high index-contradict element method, such as Si/SiO2, enables to minimize photonic-device dimensions. To increase the electric field increment at the slot interfaces in the slot-waveguides sensors. Slot waveguides for highly sensitive and lightweight biochemical integrated optical sensing, the theoretically investigated of the silicon-on-insulator. [68]

The main device of our interest consists of two separate silicon cores. The silicon on insulator (SOI) slot-waveguide modal use has been inquire into by full 2D FEM. The geometric parameters include the core width and slot width both determine by the lithograph and he height of the waveguide. Air, water, glass and others low index material can be used for the cladding material. We are use silicon oxide as the cladding material in this work. [69]
The refractive index silicon (1.33), silicon oxide (3.47) and salinity (1.35) respectively. Finally, the device dimension has been consider can be the silicon core of height H= 150 μm,, width W=100μm,slot width Ws=100μm and wavelength 1550nm. After the simulation we get 1.358 effective mode index.

Table 5.1: Parameters for Salinity in a slot waveguide

Wavelength(wl)	1550 nm
Height (H)	150 µm
Core width(W)	100 µm
Slot width(Ws)	100 µm
Frequency(fo)	C_const/wl

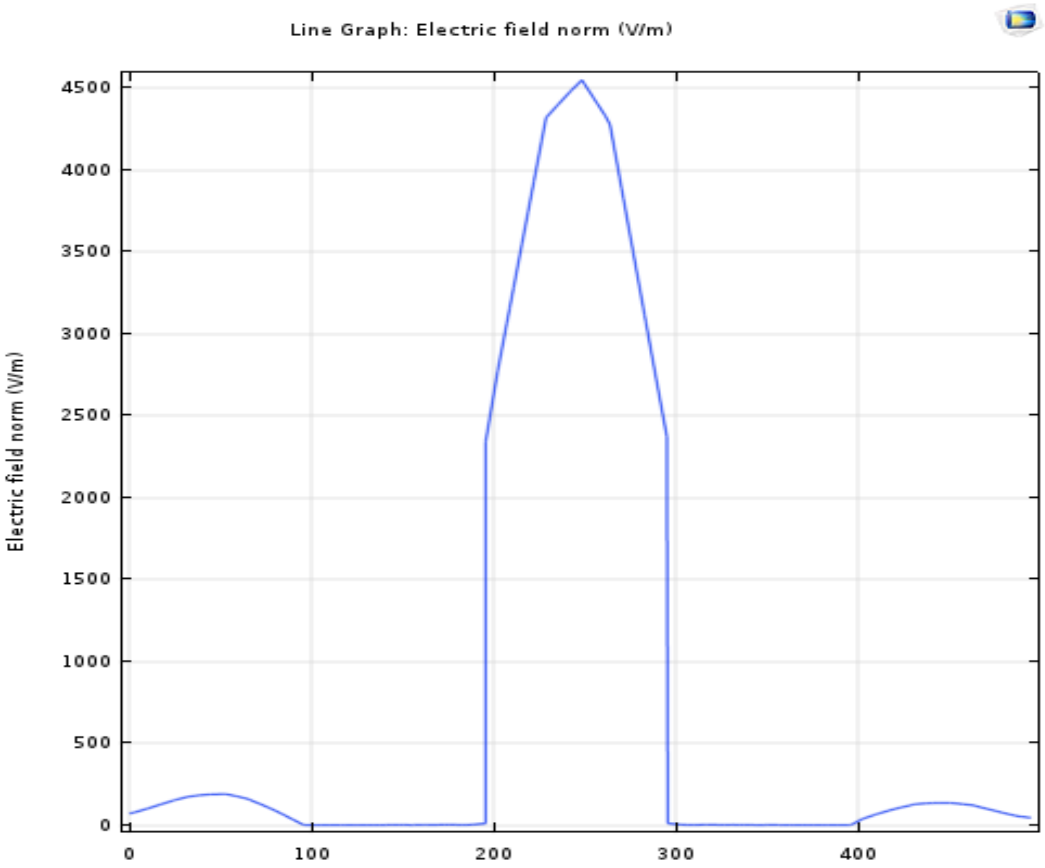

Fig 5.2: Line graph for simulation of salinity

Electrical field strength in X direction in the slot .same field are also generate in outside the slot like this so a negligible pic was appear there are fundamental mode. The X direction magnitude variation in the electric field that is soon the next image. We will try order in the higher mode they are salinity so have measure in the refractive index and curve is linear. There are any point arbitrary salinity for refractive index. We can measure in the refractive index in the sea water.

Simulation of a slot waveguide as a Water sensor:

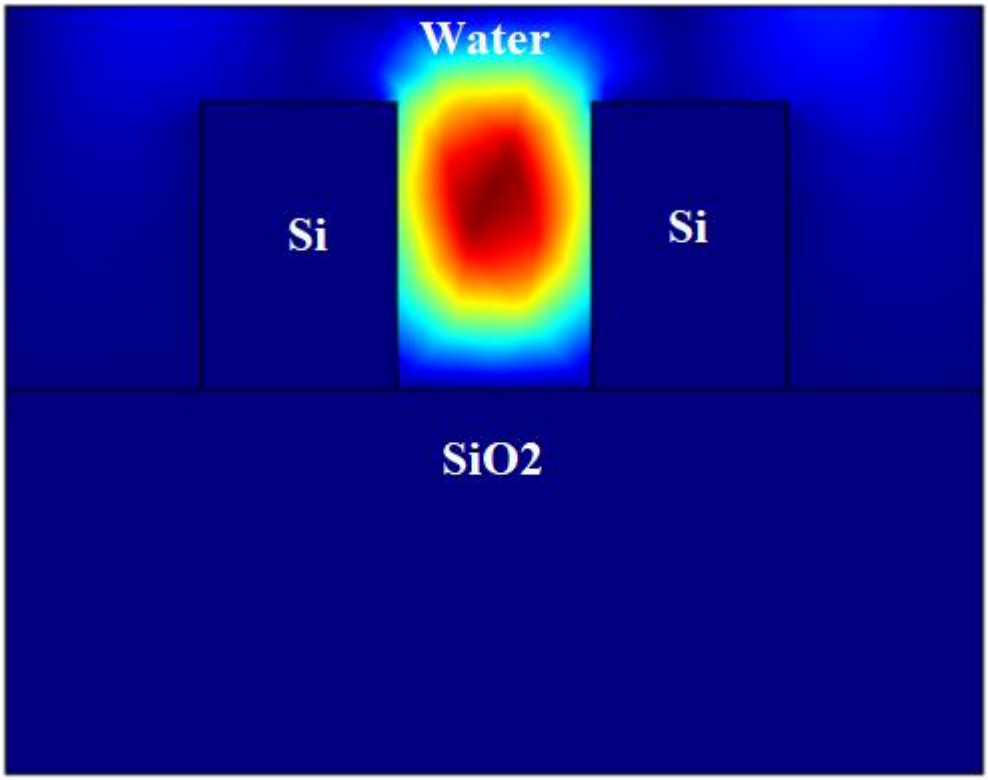

Fig 5.3: Simulation of Water in a slot waveguide

In this simulation we can see the enhancement electric field into slot region for optimized device dimension. For this simulation, uses materials are silicon, silica glass and water. We used the refractive index of silicon 3.48, refractive index of silicon oxide 1.45 and refractive index of water 1.33. Here, we used silicon strip width W=100µm, silicon strip height H=150µm, and slotted region width W_s=100µm. Here, we used 2D Finite Element Method code for this simulation. After the simulation we get 1.333 effective mode index.

Table 5.2: Parameters for water in a slot waveguide.

Wavelength(wl)	1550 nm
Height (H)	150 µm
Core width(W)	100 µm
Slot width(Ws)	100 µm
Frequency(fo)	C_const/wl

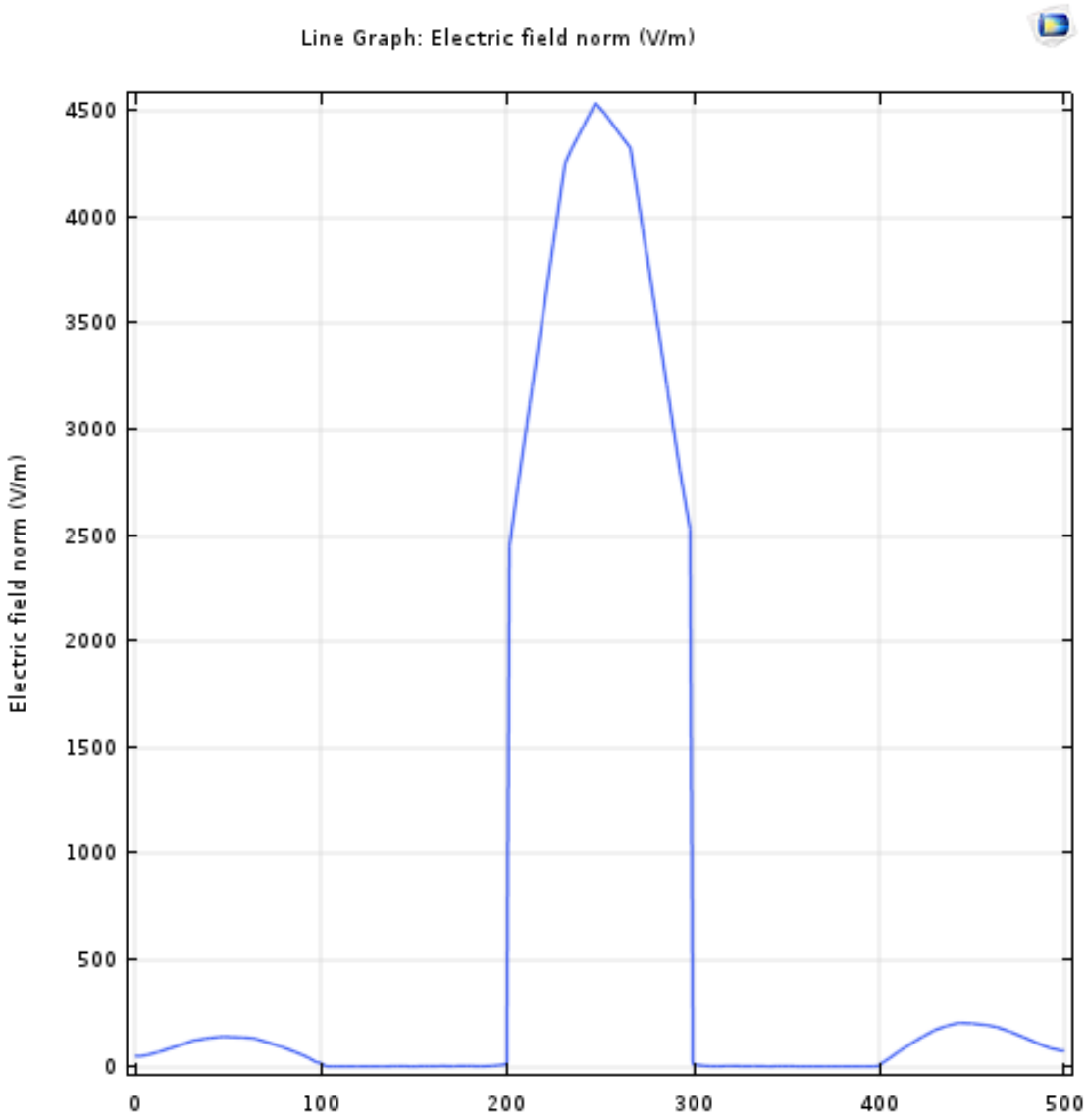

Fig 5.4: Line graph Simulation of water

Electrical field strength in X direction in the slot .same field are also generate in outside the slot like this so a negligible pic was appear there are fundamental mode. The X direction magnitude variation in the electric field that is soon the next image. We will try order in the higher mode they are water so have measure in the refractive index and curve is linear. There are any point arbitrary water for refractive index. We can measure in the refractive index in the water.

Simulation of a slot waveguide as an Air sensors:

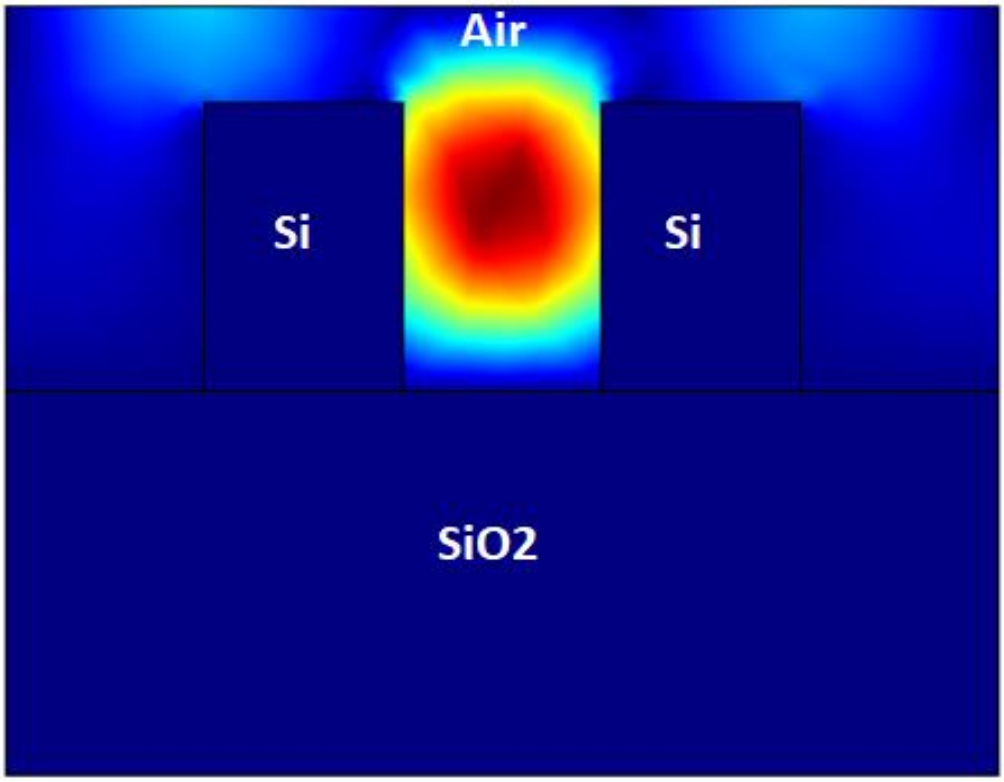

Fig 5.5: Simulation of Air in a slot waveguide

The investigation is based on homogeneous bio-sensing, where we found both the strip and the slot area to be a dense bio-ad layer. The air fills the slot region and the cover medium and only cover medium is filled with investigate solution and air bubble the narrow slot region. The silicon slot waveguide is separate by a silicon dioxide buffer layer from the silicon substrate. For this simulation, using materials are silicon, silica glass and air. The silicon and silicon dioxide refractive index from the Nsi=3.47, Nsio2=1.44 and air refractive index Nair=1 respectively. Here we are used silicon core of height H= 150 μm, width W=100μm, slot width Ws=100μm and wavelength 1550nm. After the simulation we get 0.9999 effective mode index

Table 5.3: Parameters for Air slot waveguide

Wavelength(wl)	1550 nm
Height (H)	150 µm
Core width(W)	100 µm
Slot width(Ws)	100 µm
Frequency(fo)	C_const/wl

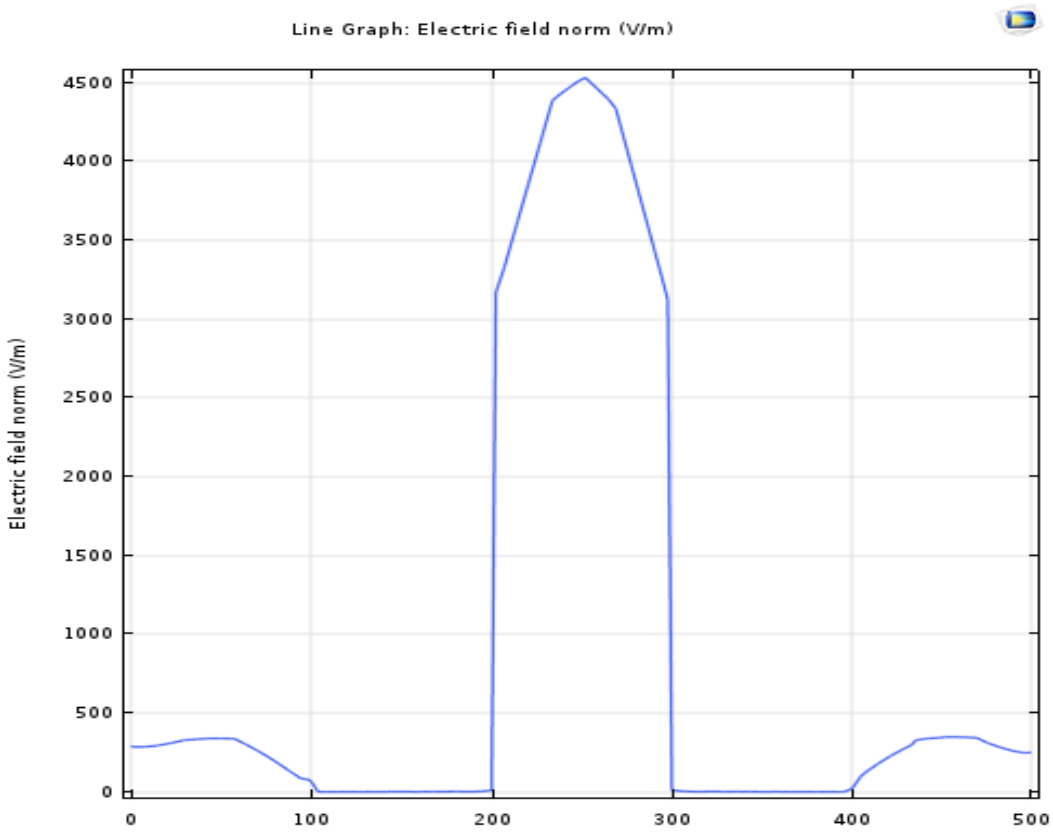

Fig 5.6: Line graph for simulation of Air

Electrical field strength in X direction in the slot .same field are also generate in outside the slot like this so a negligible pic was appear there are fundamental mode. The X direction magnitude variation in the electric field that is soon the next image. We will try order in the higher mode they are salinity so have measure in the refractive index and curve is linear. There are any point arbitrary salinity for refractive index. We can measure in the refractive index in the sea water.

Simulation of**:** a slot waveguide as an Air sensor **(**nm**):**

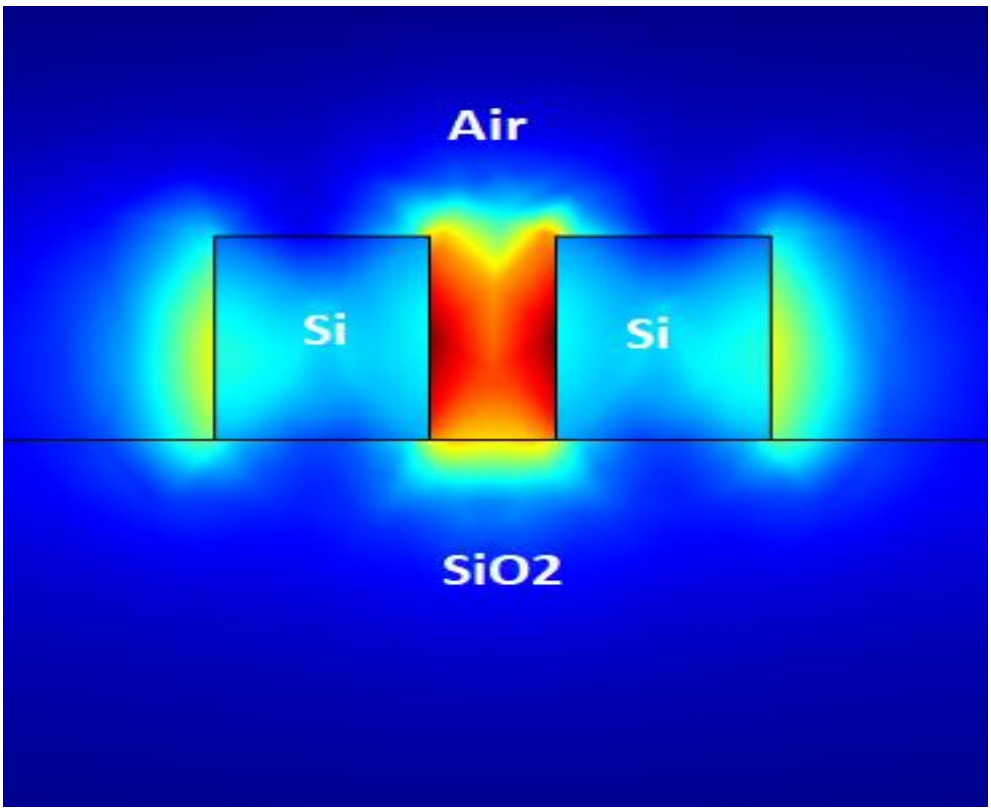

Fig 5.7: Simulation of Air (nm) in a slot waveguide

Table 5.4: Parameters for Air (nm) slot waveguide:

Wavelength(wl)	1550 nm
Height (H)	220 nm
Core width(W)	170 nm
Slot width(Ws)	100 nm
Frequency(fo)	C_const/wl

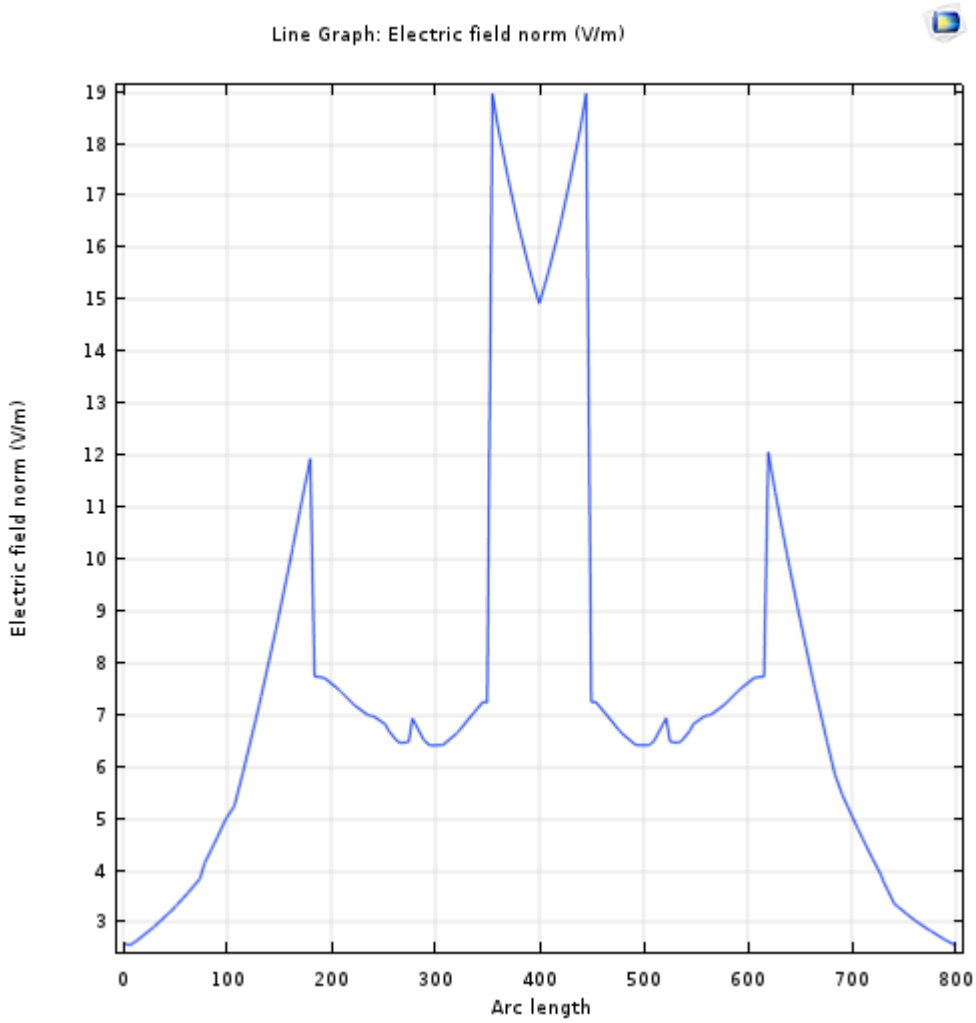

Fig 5.8: Line graph for simulation of Air (nm)

Simulation of a slot waveguide as a Carbon dioxide sensor:

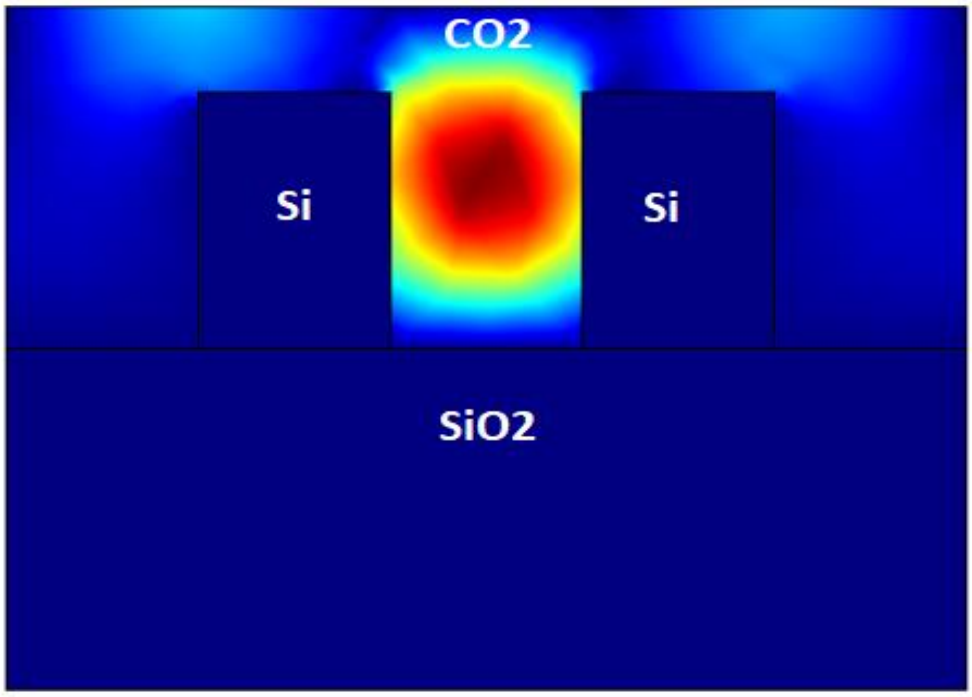

Fig 5.9: Simulation of Carbon dioxide gas in a slot waveguide

We designed Silicon slot waveguide-based sensors considering the overlap of bio-layer with lightweight propagation section so as to appreciate specific gas detection with higher sensitivity. We detected CO2 by fabricated Silicon slot waveguide ring resonators with the difference of refractive index and sensitivity. That means the device fulfil detection capability and compatibility with bio-layer toward specific gas sensing. For this simulation, using materials are silicon, silica glass and CO2. We used the refractive index of silicon 3.48, refractive index of silicon oxide 1.45 and refractive index of Carbone dioxide 1.00044. Here, we used silicon strip width W=100µm, silicon strip height H=150 µm, and slotted region width W_s=100 µm. Here, we used 2D Finite Element Method code for this simulation. After the simulation we get 1.0004 effective mode index.

Table 5.5: Parameter for Carbon dioxide in the slot waveguide

Wavelength(wl)	1550 nm
Height (H)	150 µm
Core width(W)	100 µm
Slot width(Ws)	100 µm
Frequency(fo)	C_const/wl

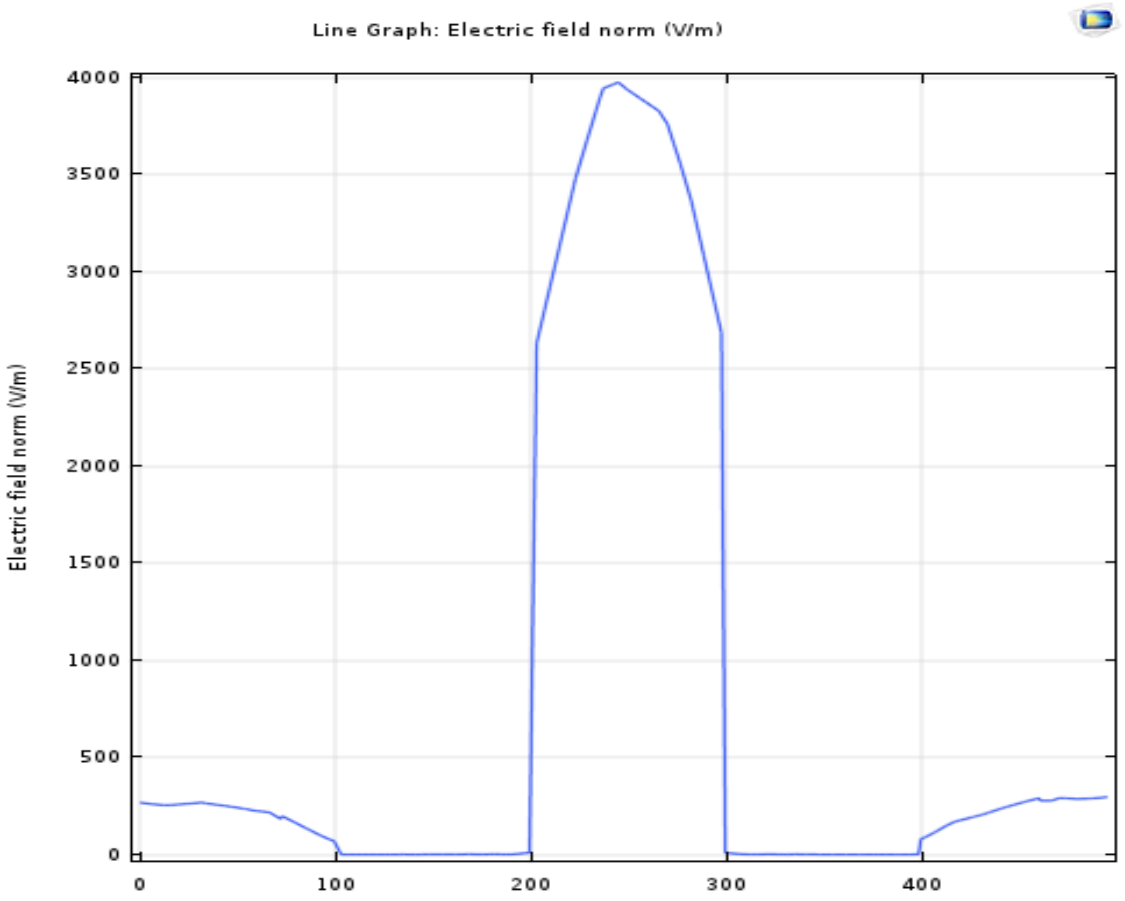

Fig 5.10: Line graph for CO_2 simulation

Electrical field strength in X direction in the slot .same field are also generate in outside the slot like this so a negligible pic was appear. There are fundamental mode. The X direction magnitude variation in the electric field that is soon the next image. We will try order in the higher mode they are carbon dioxide so have measure in the refractive index and curve is linear. There are any point arbitrary carbon dioxide for refractive index. We can measure in the refractive index in the carbon dioxide

Simulation of a slot waveguide as a Methane sensor**:**

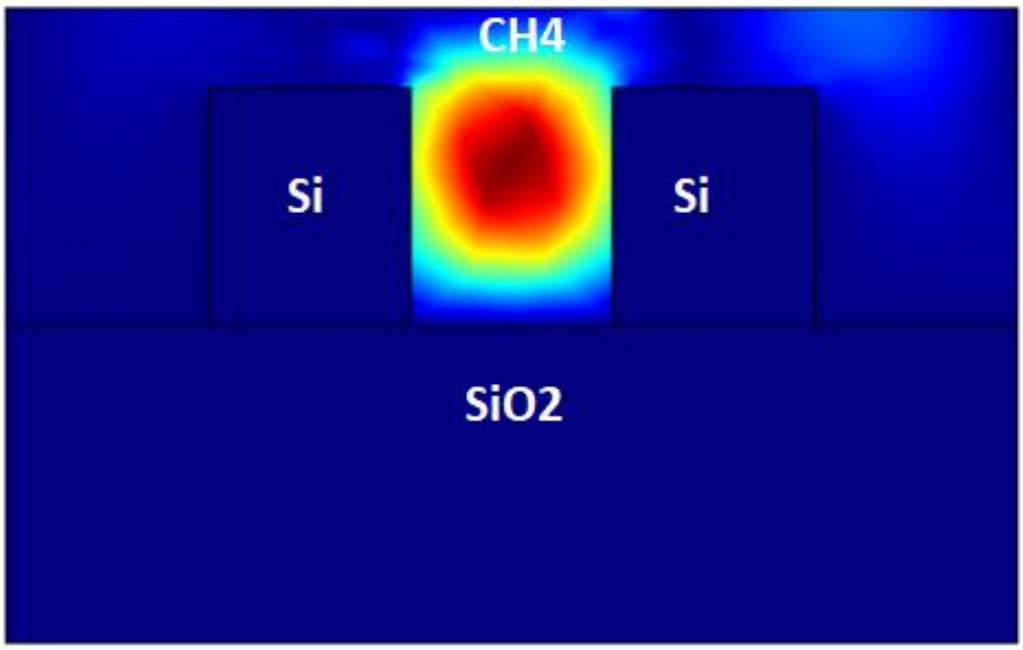

Fig 5.11: Simulation of Methane in a slot waveguide

The vertical and horizontal slot waveguides can only guide the quasi-TE and TM modes.it is also use for biochemical sensing which for both TE and TM modes supports the much stronger field development in the slot region. A much Zehnder interferometer could be used to assess the active index shift during the phase of methane sensing. There are consist of two separate core.We are use silicon dioxide as the cladding material in thiswork.in this simulation, we are used materials are silicon, silica glass and methane. We used the refractive index of silicon 3.48, refractive index of silicon oxide 1.45 and refractive index of methane 1.273 Here, we used silicon core width W=100µm, silicon core height H=150 µm, slot region widt h W_s=100 µm and wavelength 1550nm. Here, we used 2D Finite Element method in this simulation. After the simulation we get 1.273 effective mode index.

Table 5.6: Parameters Methane in the slot waveguide.

Wavelength(wl)	1550 nm
Height (H)	150 µm
Core width(W)	100 µm
Slot width(Ws)	100 µm
Frequency(fo)	C_const/wl

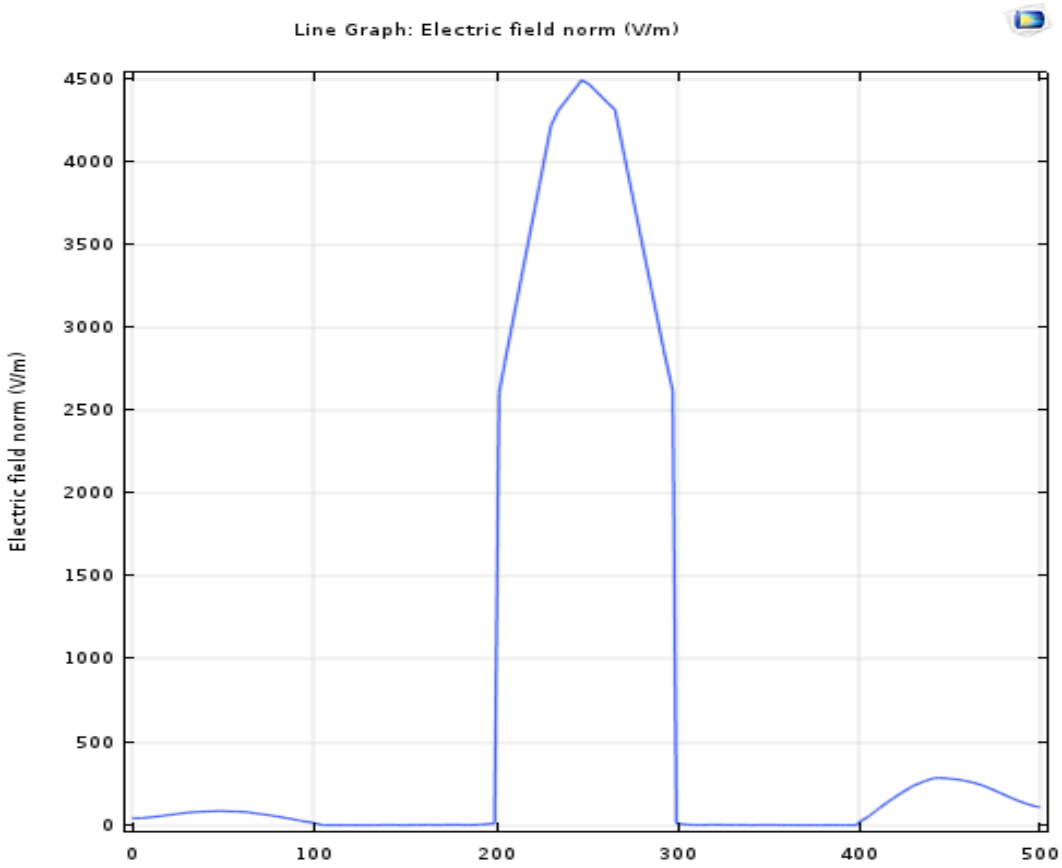

Fig 5.12: Line graph for simulation of methane

Electrical field strength in X direction in the slot .same field are also generate in outside the slot like this so a negligible pic was appear there are fundamental mode. The X direction magnitude variation in the electric field that is soon the next image. We will try order in the higher mode they are methane so have measure in the refractive index and curve is linear. There are any point arbitrary methane for refractive index. We can measure in the refractive index in the methane.

Refractive index variation with salinity:

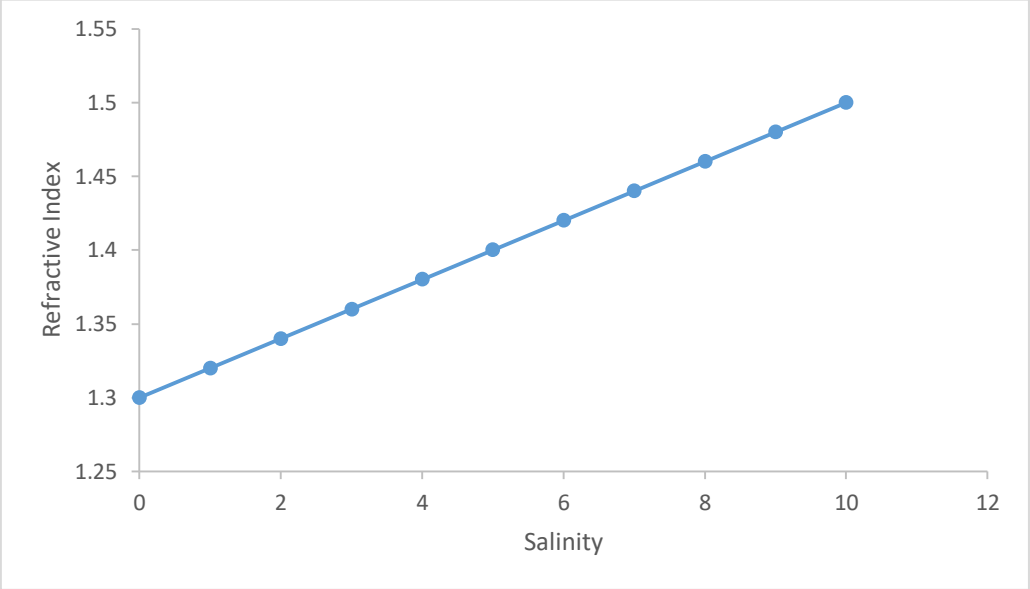

Fig 5.13: Refractive index variation with salinity

A low-cost, high-sensitivity optical fiber sensor is theoretically studied and experimentally verified for detection of salinity. The refractive index is 1.3525 are, respectively, obtained for different detection methods with respect to the change of NaCl concentration. The experimental results also indicate that the sensor introduced is capable of measuring refractive index continuously. The Salinity is an important material of natural water and industrial waste of water. Salinity detection and measurement were extensive applications and the high realistic sharpness in ocean environment protection, ocean quality, water source quality, and concrete structures. Electrical conductivity is a parameter that is widely used to test liquid salinity. Its relation to the dissolved salt mass is subject to a number of other variables and uncertainty. The ionic substances in the solution may have different conductivity from the sodium chloride salt solution. The most widely used refractive index measurement system based on the critical angle of the optical prism analytic. Salinity of the seawater is a measurement of the concentration of dissolved salts which are the mainly sodium chloride but the include salts involving magnesium, sulfur, calcium and potassium. The evaporation rate is high, so it is salinity and the inflow of freshwater is high, so its salinity is low. The ocean currents contribute to the salinity variations. The Salinity of temperature and density of water are correlative. At any change in the temperature and density influences the salinity of an area. The amount of refraction, referred to the refractive index is influenced by both the salinity and temperature of the water. The refractive index increased with increasing salinity and decreasing temperature.

Refractive index variation with wavelength:

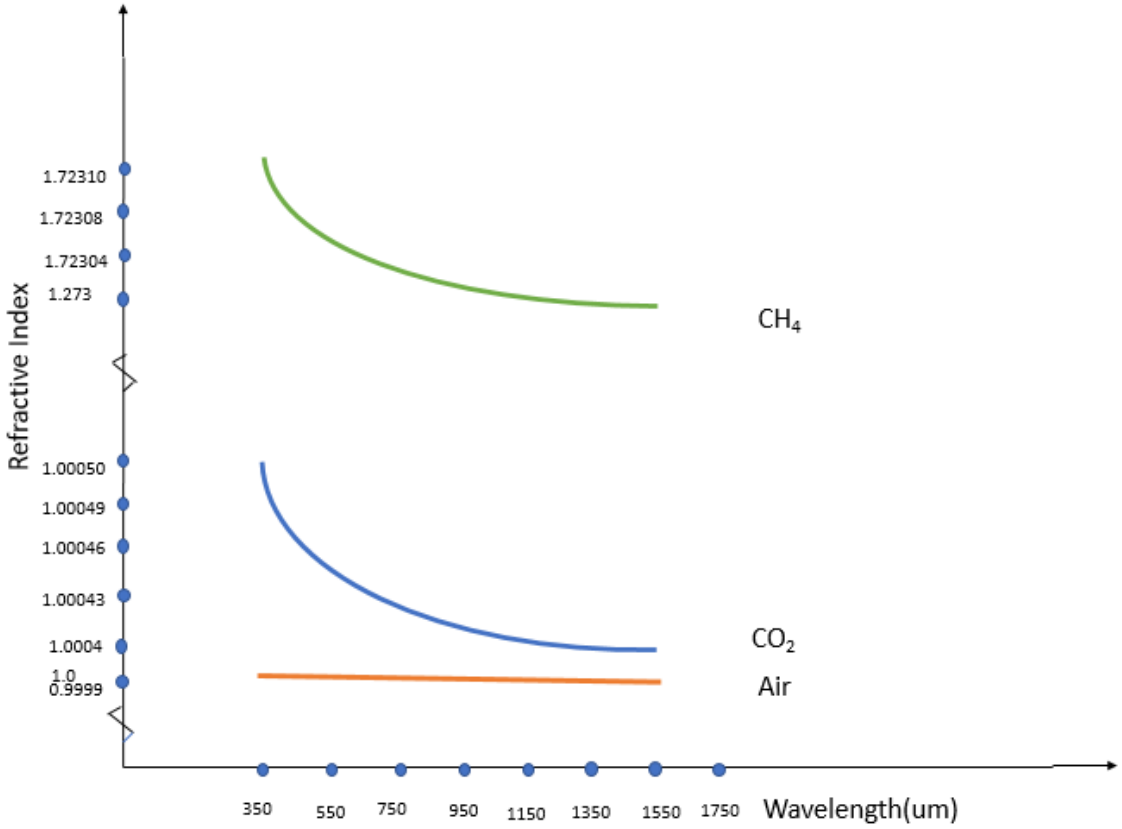

Fig 5.14: Air, Carbon dioxide and methane refractive index variation with wavelength

The refractive index most transparent materials is slightly depend on the wavelength .v is the velocity in the medium. The refractive index is inversely proportion to the wavelength .the wavelength is high refractive index is low. The wavelength is low refractive index is high. The wavelength is change but air refractive index is no change. Air effective index mode is constant but carbon dioxide and methane refractive index is change.

We know, $n=\frac{C}{vm}$ here, n=Effective mode

C=velocity of light

Vm=velocity of materials

In this equation we see that effective mode of material depends on velocity of material. When velocity of materials is increase then effective mode of materials is decrees. Here velocity of air is high so we get the refractive index of materials low and it was 0.9999. Velocity of CO_2 is lower than water so we get refractive index of CO2 is higher than water and was 1.0004. We get highest refractive index for methane because density of methane lowest. For methane we get refractive index 1.723.

Chapter 6
Conclusion and Future Work

In this thesis, we mainly emphasized on silicon slot waveguide based sensors. We tried to measure the effective refractive index of the guided mode in the slot waveguide to detect the environment in between the slot of Si slabs on SiO_2 substrate. As specificity, the difference in effective index were used to detect different gases, especially CO_2, methane and also used to detect the level of salinity of sea water. We also provided the comparison between how at different environment the fundamental guided mode in the silicon slot waveguide may vary. In countries those faces severe winter season, the people usually most of the time keep the windows and ventilators closed to survive. Which increases the CO_2 level in their house and this condition may become fetal to the infants of the house. In western countries death toll in such environment is not negligible at all. Optical sensors can easily detect the increasing level of CO_2 concentrations and may save lives. Our country earn a lot profit from Prawn cultivation. Farmers those cultivate prawn they should maintain salinity level for their prawn pond. Because prawns cannot survive with low or high salinity level. If salinity level increases in our prawn pond, then we face complication and losses. So we need to control salinity level in our prawn pond. We can control salinity level by using optical sensors. We used Si-slot waveguide optical sensors to detect presence of CO_2 in air, CH_4 in air, to detect level of salinity in sea water and also detecting molecule in medical test sector. In this thesis we have simulated and analyzed fundamental mode of silicon slot waveguide using Comsole Multiphysics simulation software.

In future we will apply the similar types of concept on sound system technology.

References:

1. URL: https://en.wikipedia.org/wiki/Photonics Access date:20th August

2.URL:https://encryptedtbn0.gstatic.com/images?q=tbn:ANd9GcS4wxg4Yw6wQW4C8M45ui51qboX7Xxbju1jeCfeSSlB967R-jLp-g&s Access date:20th August

3. URL:https://www.elprocus.com/diffrent-types-of-fiber-optic-sensors/

Access date:20th August

4. URL: https://en.wikipedia.org/wiki/Fiber-optic_sensor Access date:20th August

5.URL:http;//ecomputernotes.com/computernetworkingnotes/communication networks/optical-source Access date:20th August

6. URL:"Optical Fiber". *www.thefoa.org.* "The Fiber Optic Association". Retrieved 17 April 2015. Access date: 21th August

7. URL:https://en.wikipedia.org/wiki/Transducer Access date: 21th August

8. Jack Ready "Optical Detectors and Human Vision"

9. URL:https://whatis.techtarget.com/definition/oscilloscopeAccess date: 21th August

10. URL: https://www.azosensors.com/article.aspx?ArticleID=333Access date: 21th August

11. URL:https://www.mdpi.com/journal/sensorsAccess date: 22th August

12. URL:https://www.ncbi.nlm.nih.gov/pubmed/19532747Access date: 22th August

13.URL:https://www.kth.se/polopoly_fs/1.451034.1550158638!/Menu/general/columncontent/attachment/gylfason_silicon_photonics_biosensing.pdfAccess date: 22th August

14. Ghosh, S. and Rahman, B. M. "An Innovative Straight Resonator Incorporating a Vertical Slot as an Efficient Bio-Chemical Sensor" IEEE Journal on Selected Topics in Quantum Electronics (2016).

15.URL:https://www.researchgate.net/publication/311241866_A_MetalAssisted_Silicon_Slot_Waveguide_for_Highly_Sensitive_Gas_DetectionAccess date: 22th August

16. Tom Claes Jordi and Gironès Molera and Katrien De Vos and Etienne Schacht and Roel Baets Peter Bienstman "Label-Free Biosensing With a Slot-Waveguide-Based Ring Resonator in Silicon on Insulaton" Volume 1, Number 3, September 2009

17. URL:https://www.osapublishing.org/abstract.cfm?uri=CLEO_AT-2019-JTh2A.96

Access date: 23th August.

18. Chao Pan and B. M. A. Rahman "High-Sensitivity Polarization-Independent Biochemical Sensor Based on Silicon-on-Insulator Cross-Slot Waveguide"

19. URL:https://en.wikipedia.org/wiki/Slot-waveguide Access date: 24th August

20.URL:https://pdfs.semanticscholar.org/30d1/37535c59e322a8dc8c3d222cfa2e0763d9f1.pdf Access date:5th August,2019

21. Zienkiewitz, "The Finite Element Method", New York, McGraw-Hill, 1973.

22. M.V.K. Chari and P.P. Silvester, "Finite Elements in Electrical and Magnetic Field Problems", Chechester, Wiley, 1980

23. E. Yamashita, Analysis Methods for "Electromagnetic Wave Problems" (Boston, Artech House,1990)

24. D.B. Davidson, "Computational Electromagnetics for RF and Microwave Applications" (Cambridge, Cambridge University Press, 2005)

25. URL: https://cds.cern.ch/record/1698084/files/1580538320_TOC.pdfAccess date: 14th October,2019

26. URL:https://www.semanticscholar.org/paper/Improved-Complex-Envelope-Method-for-Cavities-Pinto-Obayya/3e6558caca467d59d9a5168e6bf8d3e3dd7e3f07

Access date:20th October,2019

27.URL:https://pdfs.semanticscholar.org/1502/c6a1b0b211502f7a6641d127843fcca486cb.pdfAccess date:8th November,2019

28.B.M. Azizur Rahman, "Finite-element analysis of optical and microwave waveguide problems".IEEE Trans. Microwave Theor. Techniq. 32(1), 20–28 (1984)

29.URL:http://s2.bitdl.ir/Ebook/Physics/Physics%20Complete/Modern%20Physics/Quantum%20Mechanics/Introduction%20to%20Optical%20Waveguide%20Analysis%20Solving%20Maxwell%27s%20Equation%20and%20the%20Schrdinger%20Equation%20%20Kenji%20Kawano,%20Tsutomu%20Kitoh.pdf Access date:2nd November,2019

30. M. Koshiba and H. Saitoh, M. Eguchi and K. Hirayama, "Simple scaler finite element approach to optical waveguides". IEE Proc. J. 139, 166–171 (1992)

31. S.S.A. Obayya, "Computational Photonics"(Wiley, 2011)

32. S.S.A. Obayya, "Efficient finite-element-based time-domain beam propagation analysis of Optical integrated circuits". IEEE J. Quant. Electron. 40(5), 591–595 (2004)

33.URL:http://citeseerx.ist.psu.edu/viewdoc/download?doi=10.1.1.830.251&rep=rep1&type=pdf Access date:2nd November,2019

34. A. Abdrabou and A.M. Heikal and S.S.A. Obayya, "Efficient rational Chebyshev pseudo-spectral method with domain decomposition for optical waveguides modal analysis". Opt. Express 24(10), 10495–10511 (2016)

35. D.M. Pozar, "Microwave Engineering" (Wiley, Hoboken, NJ, 2012)

36. URL:https://www.sciencedirect.com/science/article/pii/S0021999184711594

37. S.D. Gedney, “An anisotropic perfectly matched layer absorbing media for the truncation of FDTD latices.” Antennas Prop. IEEE Trans. 44, 1630–1639 (1996)

38. URL:https://web.stanford.edu/class/ee256/ChewWeedon.pdf

Access date: 7th November, 2019

39. W.C. Chew, J.M. Jin, E. Michielssen, “Complex coordinate stretching as a generalized absorbing boundary condition. Microwave Opt”. Technol. Lett. 15(6), 363–369 (1997)

40. URL: https://eprints.lib.hokudai.ac.jp/dspace/bitstream/2115/5585/1/JLT18-1.pdf

Access date: 10th November, 2019

41. V.F. Rodríguez-Esquerre and M. Koshiba, “Finite element analysis of photonic crystal cavities: time and frequency domain. J. Lightwave Technol”. 23(3), 1514–1521 (2005)

42.URL:https://pdfs.semanticscholar.org/30d1/37535c59e322a8dc8c3d222cfa2e0763d9f1.pdf Access date:10th November,2019

43.V.F. Rodríguez-Esquerre and M. Koshiba and E.H.-Figueroa, “Frequency-dependent envelope finite element time domain analysis of dispersion materials. Microwave Opt. Tech”. Lett.44(1),13–16(2004)

44.URL:https://www.researchgate.net/publication/3242921_Finiteelement_analysis_of_photonic_crystal_cavities_Time_and_frequency_domainAccess date: 12th November,2019

45. G.R. Liu “A Generalized gradient smoothing technique and the smoothed bilinear form for Galerkin formulation of a wide class of computational methods”. Int. J. Comput. Methods (2008)

46. K.S.R. Atia and S.S.A. Obayya, “Novel gradient smoothing method-based time domain beam propagation analysis of optical integrated circuits. Signal Process”. Photon. Commun. JM3A–23(2015)

47. G.R. Liu, “Meshfree Methods: Moving Beyond the Finite Element Method” (CRC Press, 2009)

48. J.R. LeVeque, “Finite Volume Methods for Hyperbolic Problems” (Cambridge,2002)

49.URL:https://books.google.com.bd/books?id=zv1fDwAAQBAJ&pg=PA150&lpg=PA150&dq=K.S.R.+Atia,+A.M.+Heikal,+S.S.A.+Obayya,+Efficient+smoothed+finite+element+time+domainbeam+propagation+method+for+photonic+devices.+Opt.+Exp.+23(17),+22199%E2%80%9322213+(2015)&source=bl&ots=FfCgY8Tnx4&sig=ACfU3U02ELcJbth5x0SZFcwr7R_GcJI08Q&hl=en&sa=X&ved=2ahUKEwizv2JlZfmAhVbb30KHbU7DYkQ6AEwAXoECAoQAQ#v=onepage&q&f=false Access date:14th November,2019

50.K.S.R. Atia and A.M. Heikal and S.S.A. Obayya, “Time-domain beam propagation method based on gradient smoothing technique for dispersive materials”, in Progress in Electromagnetics Research symposium (PIERS) (2015)

51.URL:https://www.photonics.intec.ugent.be/download/pub_2476.pdf

Access date:15th november,2019

52. G.H. Jin and J. Harari, J.P. Vilcot and D. Decoster, “An improved time domain beam propagation method for integrated optics components”. IEEE Photon. Technol. Lett. 9(3), 117–122 (1997)

53. J. Lee and B. Fornberg, “A split step approach for the 3-D Maxwell’s equations”. J. Comput. Appl.Math. 158(2), 485–505 (2003)

54. M.F.O. Hameed and Y.K.A. Alrayk, S.S.A. Obayya, “Self-calibration highly sensitive photo nic crystal fiber biosensor”. IEEE Photon. 8(3) (2016)

55.URL:https://ieeexplore.ieee.org/stamp/stamp.jsp?arnumber=7447655

Access date: 17th November,2019

56. S.I. Azzam and R.E.A. Shehata and M.F.O. Hameed, A.M. Heikal, S.S.A. Obayya, “Multichannel photonic crystal fiber surfrace plasmon resonance based sensor”. J. Opt. Quant. Electron. 48(142) (2016)

57. URL:https://www.osapublishing.org/DirectPDFAccess/C7C38B2D-0C82-1E7F-E66060E86B93871A_324086/oe-23-17-22199.pdf?da=1&id=324086&seq=0&mobile=no

Access date:17thNovember,2019

58. M.F.O. Hameed and S.S.A. Obayya and H.A. El-Mikati, “Passive polarization converters based onphotonic crystal fiber with L-shaped core region”. IEEE J. Lightwave Technol. 50(6) (2012)

59. M.F.O. Hameed, A.M. Heikal, S.S.A. Obayya, “Novel passive polarization rotator based on spiral photonic crystal fiber”. IEEE Photon. Technol. Lett. 25(16) (2013)

60. M.F.O. Hameed, S.S.A. Obayya, R.J. Wiltshire, “Beam propagation analysis of polarization rotation in soft glass nematic liquid crystal photonic crystal fibers”. IEEE Photon. Technol.Lett. 22(3) (2010)

61. M.F.O. Hameed and A.M. Heikal, S.S.A. Obayya, “Passive polarization converters based on photonic crystal fibers”. IEEE Photon. Technol. Lett. 22(3) (2010)

62. S.I. Azzam and M.F.O. Hameed and N.F.F. Areed and S.S.A. Obayya and H. El-Mikati et al., Proposal of ultracompact “CMOS compatible TE-/TM-pass polarizer based on SOI platform”. IEEE Photon.Technol. Lett. 33(13) (2015)

63. A.M. Heikal and F.F.K. Hussain and M.F.O. Hameed and S.S.A. Obayya, “Efficient polarization filter design based on plasmonic photonic crystal fiber”. IEEE J. Lightwave Technol. 33(13) (2015)

64. S.S.A. Obayya and M.F.O. Hameed and N.F.F. Areed, “Computational Liquid Crystal Photonics: Fundamentals” (Wiley, Modelling and Applications, 2016)

65. M.F.O. Hameed, S.S.A. Obayya, K. Al-Begain, A.M. Nasr, M.L. Abo el Maaty, “Coupling characteristics of a soft glass nematic liquid crystal photonic crystal fiber coupler”. IETOptoelectron. 3(6) (2009)Access date:19th november,2019

66. M.F.O. Hameed and A.M. Heikal and B.M. Younis and M.M. Abdelrazzak and S.S.A. Obayya, “Ultra-high tunable liquid crystal plasmonic photonic crystal fiber polarization filter”. Opt. Exp. 23(6),7007–7020 (2015)

67. URL:https://en.wikipedia.org/wiki/COMSOL_MultiphysicsAccess date:19th July 2019

68. URL:https://www.mdpi.com/1424-8220/9/6/4751/htmAccess date:19th november,2019

69. URL:https://www.osapublishing.org/oe/abstract.cfm?uri=oe-21-16-19029)

Access date:19th november,2019

70.URL:http://openaccess.city.ac.uk/id/eprint/16546/1/Souvik_IEEEJSTQEfinalsubmission2016.pdf%20Access%20date:%201st%20December,2019 Access Date :1st November